GSK1702934A and M085 directly activate TRPC6 *via* a mechanism of stimulating the extracellular cavity formed by the pore helix and transmembrane helix S6

Received for publication, April 9, 2021, and in revised form, August 22, 2021 Published, Papers in Press, August 28, 2021,
https://doi.org/10.1016/j.jbc.2021.101125

Pei-Lin Yang[1,‡], Xing-Hua Li[1,‡], Jin Wang[2,‡], Xue-Fei Ma[3], Bo-Ying Zhou[2], Yuan-Feng Jiao[2], Wen-Hui Wang[2], Peng Cao[4], Michael Xi Zhu[5], Pei-Wang Li[6], Zhi-Hong Xiao[6], Chang-Zhu Li[6], Chang-Run Guo[1,*], Yun-Tao Lei[7,*], and Ye Yu[2,*]

From the [1]School of Traditional Chinese Pharmacy, [2]Department of Basic Medicine and Clinical Pharmacy, China Pharmaceutical University, Nanjing, China; [3]College of Bioscience and Biotechnology, Hunan Agricultural University, Changsha, China; [4]Hospital of Integrated Traditional Chinese and Western Medicine, Nanjing University of Chinese Medicine, Nanjing, China; [5]Department of Integrative Biology and Pharmacology, McGovern Medical School, The University of Texas Health Science Center at Houston, Houston, Texas, USA; [6]State Key Laboratory of Utilization of Woody Oil Resource, Hunan Academy of Forestry, Changsha, China; [7]School of Science, China Pharmaceutical University, Nanjing, China

Edited by Mike Shipston

Transient receptor potential canonical (TRPC) channels, as important membrane proteins regulating intracellular calcium (Ca^{2+}_i) signaling, are involved in a variety of physiological and pathological processes. Activation and regulation of TRPC are more dependent on membrane or intracellular signals. However, how extracellular signals regulate TRPC6 function remains to be further investigated. Here, we suggest that two distinct small molecules, M085 and GSK1702934A, directly activate TRPC6, both through a mechanism of stimulation of extracellular sites formed by the pore helix (PH) and transmembrane (TM) helix S6. *In silico* docking scanning of TRPC6 identified three extracellular sites that can bind small molecules, of which only mutations on residues of PH and S6 helix significantly reduced the apparent affinity of M085 and GSK1702934A and attenuated the maximal response of TRPC6 to these two chemicals by altering channel gating of TRPC6. Combing metadynamics, molecular dynamics simulations, and mutagenesis, we revealed that W679, E671, E672, and K675 in the PH and N701 and Y704 in the S6 helix constitute an orthosteric site for the recognition of these two agonists. The importance of this site was further confirmed by covalent modification of amino acid residing at the interface of the PH and S6 helix. Given that three structurally distinct agonists M085, GSK1702934A, and AM-0883, act at this site, as well as the occupancy of lipid molecules at this position found in other TRP subfamilies, it is suggested that the cavity formed by the PH and S6 has an important role in the regulation of TRP channel function by extracellular signals.

TRPC (transient receptor potential canonical) channels are known as receptor-operated, nonselective cation channels (1–3). TRPCs have been considered as potential therapeutic targets in various pathological conditions, such as cardiovascular dysfunction (4), endocrine (5), neuronal (6) and chronic kidney diseases (7), pain (8), and cancer (9). M085, also known as 4o, is a potent and selective TRPC3/6/7 activator with an EC_{50} value (the concentration yielding half maximum response) of 4.66 ± 0.03 μM, measured by patch-clamp rather than calcium imaging method (10). Other TRPC3/6/7 activators include GSK1702934A (11), which has been used to study cardiac contractility and arrhythmogenesis in the heart (12). SKF-96365, as a general TRPC antagonist, was used in the study of cardiovascular disease (13, 14). BI 749327, a selective inhibitor of TRPC6, reduces the ventricular dilation and fibrosis caused by hemodynamic stress abnormalities (15). The pyrazole compound Pyr3 selectively inhibits TRPC3 channels and prevents stent-induced arterial remodeling (16, 17). Piperazine-derived compounds PPZ1 and PPZ2 activate TRPC3/6/7 and trigger Ca^{2+} signaling to promote neurite outgrowth and neuronal survival in the absence of serum (18). The study of subtype-specific agonists and antagonists of TRPC could facilitate the development of new drug therapies, such as the treatment of glomerulonephritis (19), renal fibrosis (20), pulmonary arterial hypertension (21), and certain types of tumors (22, 23).

Activation of the TRPC channel occurs mainly downstream of GPCR-$G_{q/11}$-PLCβ and the receptor tyrosine kinase coupled to PLCγ. PLC stimulates the hydrolysis of PIP_2, leading to the production of IP_3 and DAG, and IP_3-dependent Ca^{2+} release from the endoplasmic reticulum, which causes the intracellular Ca^{2+} store depletion and eventual activation of the channel (24). TRPC6 channels, on the other hand, can be directly activated by DAG, the hydrolysis product of phospholipase PLC (25). Although an increasing number of intracellular signals have been found to activate TRPC6 in recent years (25–27), the very recent cryo-electron microscopy (cryo-EM) structure of TRPC6 complexed with AM-0883, a

‡ These authors contributed equally to this work.
* For correspondence: Ye Yu, yuye@cpu.edu.cn; Yun-Tao Lei, Leiyt10@cpu.edu.cn; Chang-Run Guo, guochangrun@126.com.

novel agonist disclosed for the first time in this study (28), showed that stimulation of extracellular sites is also capable of directly activating TRPC6, which provides direct evidence for the existence of an extracellular orthosteric site.

Indeed, intracellular signaling regulatory molecules as new drug candidates or research tools must first pass through the barrier of the cell membrane. Therefore, activation or modulation of TRPC6 from outside the cell can offer great advantage for drug development of this important subtype of TRP superfamily. Although the open structure of TRPC6 has unrevealed one of the extracellular orthosteric sites (28), it remains unclear whether there are other extracellular sites that are essential for the activation/regulation of TRPC6. Are the known agonists dependent on stimulation of the DAG binding site upon entry into the cell (28, 29), or do they activate TRPC6 directly extracellularly? In addition, it is unclear whether GSK1702934A and M085 activate TRPC6 independently of the pocket formed between the pore helix (PH) and transmembrane (TM) helix S6 (AM-0883's site) and whether there are other novel modes of extracellular regulation of TRPC6.

To explore these questions, here, *via* a combination of mutagenesis, covalent modification on TRPC mutant, whole-cell and single channel recordings, surface expression analysis, conventional molecular dynamics (CMD) simulations, metadynamics (MetaD), and free energy reconstruction, we found that although chemical structures of GSK1702934A and M085 are very different, they both activate TRPC6 *via* a mechanism of stimulating the extracellular site formed by the PH and TM helix S6, similar to the mechanism of AM-0883 revealed by the open structure of TRPC6 (28). Our findings also imply that among several small molecule binding pockets in the extracellular domain (ECD), the pocket formed by PH and S6 may be the only extracellular orthosteric site that can be activated by small-molecule agonist rather than large biomolecules (*e.g.*, toxins).

Results

M085- and GSK1702934A-mediated activations of TRPC6 are dependent on extracellular orthosteric sites

To investigate the activation mechanism of M085 and GSK1702934A, we synthesized both compounds (see Experimental procedures), and the synthesized M085 and GSK1702934A were able to activate mouse TRPC6 (mTRPC6) at EC_{50} = 3.80 ± 0.67, 0.78 ± 0.16 μM, respectively (Fig. 1, *B* and *D*). Meanwhile, to more accurately predict small molecule–protein interactions, subsequent molecular simulations were based on the cryo-EM structure of human TRPC6 (hTRPC6) rather than the homology model of mTRPC6. hTRPC6-EGFP plasmid suffers from relatively low expressing efficiency in HEK293 cells, low mutagenesis success rate, and it

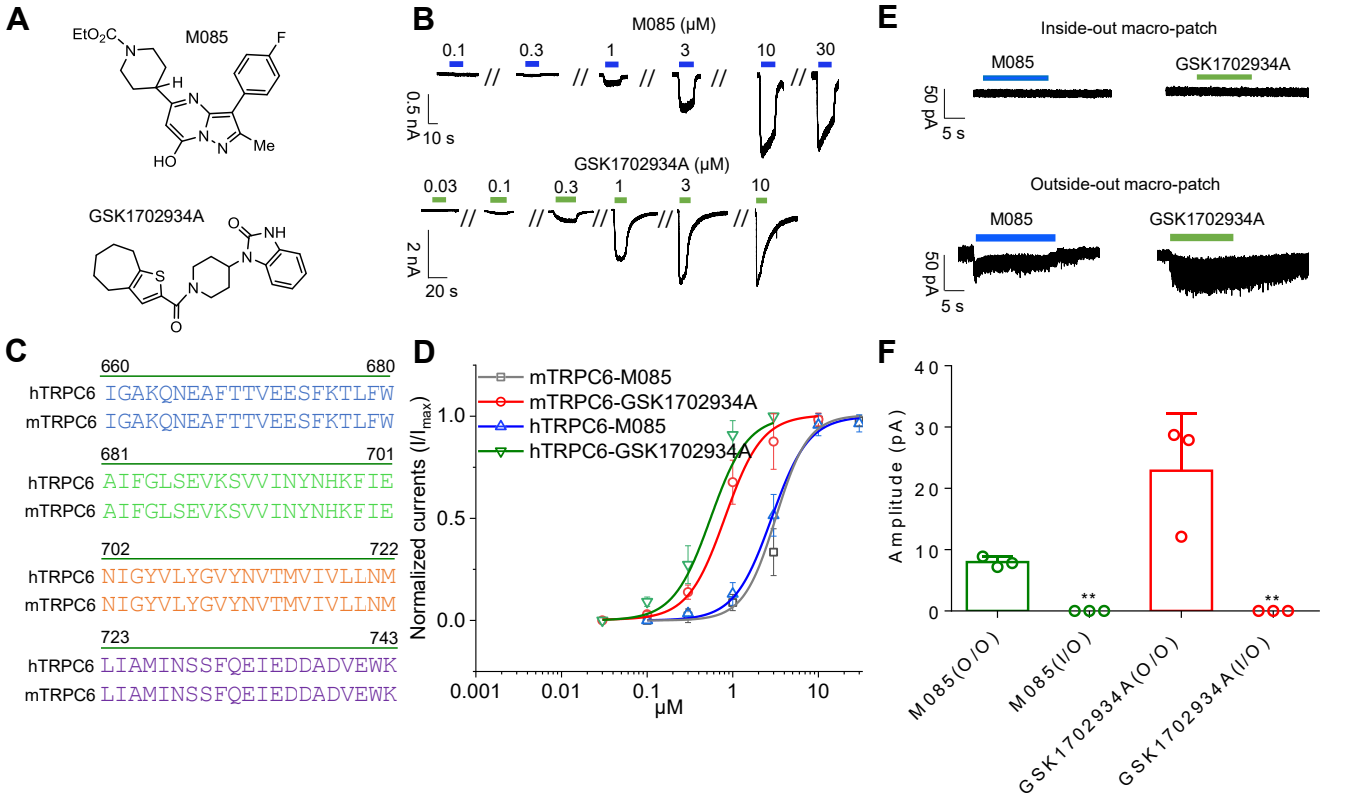

Figure 1. M085 and GSK1702934A-mediated direct activations of TRPC6 are dependent on extracellular orthosteric sites. *A*, chemical structures of M085 and GSK1702934A. *B*, representative current traces of mTRPC6 channel induced by different concentrations of M085 and GSK1702934A, respectively. *C*, pore helix and S6 sequence alignments of mTRPC6 and hTRPC6. *D*, concentration–activation curves of mTRPC6-WT and hTRPC6-WT. Each *solid line* was a fit of the Hill equation to the M085-and GSK1702934A-dependent activation (mean ± S.D., n = 3–4). *E* and *F*, typical current traces (*E*) and pool data (*F*) of M085 and GSK1702934A recorded in inside-out or outside-out macro-patch configurations. Data are presented as mean ± S.D. (n = 3). $^{**}p < 0.01$ compared with control group, Student's *t* test.

is not easy to perform electrophysiological recordings. Therefore, we adopted the following strategy: molecular simulations were based on the cryo-EM structure of hTRPC6, while mutagenesis, electrophysiological recording as well as membrane expression of mutants were validated on mTRPC6. Two points support the rationality of this strategy: 1. The sequence alignment of mTRPC6 and hTRPC6 indicates that they are highly homologous and that the amino acid sequences of the putative recognition site (see below) for these two structurally distinct small molecules are identical (Fig. 1, *A* and *C*); 2. The EC_{50} values of hTRPC6 activated by M085 and GSK1702934A are 2.94 ± 0.70 and 0.45 ± 0.03 μM, respectively, which turn out to be consistent with the corresponding EC_{50} on mTRPC6 (Fig. 1*D*).

We then examined whether the binding sites of M085 and GSK1702934A were present extracellularly or intracellularly by using the outside-out and inside-out configurations. Currents for M085 (100 μM) and GSK1702934A (100 μM) could be recorded with the outside-out configuration, while in the inside-out configuration no currents were recorded (Fig. 1, *E* and *F*), indicating that M085 and GSK1702934A-mediated activation of TRPC6 through their orthosteric sites are likely to be in the ECD of TRPC6. This result also implies that the cell membrane permeability of these two chemicals is also relatively low.

Several possibilities for the interaction of M085 and GSK1702934A with the ECD of TRPC6

We performed a scanning of small molecule binding pockets based on the cryo-EM structure of hTRPC6 and identified nine pockets including S1 to S9, of which S1, S2, and S3 are extracellular sites (Fig. 2, *A* and *B*). We focused on interactions of S1 to S3 with M085 and GSK1702934A (Fig. 2*C*), where the binding pocket S1 consists of amino acids ^{h}R464, ^{h}T488, ^{h}F491, and ^{h}Y658 (the superscript 'h' indicates hTRPC6 numbering); S2 is composed of ^{h}E672, ^{h}F675, and ^{h}W680 on the pore helix (PH), and ^{h}N702, ^{h}Y705, ^{h}V706, and ^{h}V710 on the S6 helix; S3 consists of ^{h}L685, ^{h}S686, ^{h}V688, and ^{h}K689. *In silico* docking revealed that M085 and GSK1702934A have good recognition by S1 to S3, but M085 and GSK1702934A acting on S3 are more likely to exhibit an inhibitory effect because the bound small molecule could occupy the ion permeation pathway. S1 and S2 are more likely to be binding sites for agonists.

To confirm the possibility of S1 to S3, we mutated the corresponding sites in mTPRPC6. Because M085 and GSK1702934A activate the mTRPC6 channel with the EC_{50} of approximately 5 μM and 1 μM and saturation concentrations of approximately 10 μM and 3 μM, respectively, we used the ratio of M085 activation current ($I_{10\ \mu M}/I_{5\ \mu M}$) and the ratio of GSK1702934A activation current ($I_{3\ \mu M}/I_{1\ \mu M}$) to carry out a preliminary simplified screening of the effect of different mutants in these potential binding sites on the apparent affinity of M085 and GSK1702934A. The result showed that compared with the wild-type (WT) mTRPC6 (M085-$I_{10\ \mu M}/I_{5\ \mu M}$ = 1.65 ± 0.21; GSK1702934A-$I_{3\ \mu M}/I_{1\ \mu M}$ = 1.87 ± 0.22), the mutants ^{m}R463K (the superscript 'm' indicates mTRPC6 numbering), ^{m}T487L, ^{m}F490W, and ^{m}Y657W in the S1 pocket (M085-$I_{10\ \mu M}/I_{5\ \mu M}$ = 1.54 ± 0.17, 1.26 ± 0.22, 1.91 ± 0.12, and 1.68 ± 0.24 for ^{m}R463K, ^{m}T487L, ^{m}F490W and ^{m}Y657W, respectively; GSK1702934A-$I_{3\ \mu M}/I_{1\ \mu M}$ = 1.65 ± 0.01, 1.00 ± 0.08, 1.94 ± 0.12 and 1.97 ± 0.12 for ^{m}R463K, ^{m}T487L, ^{m}F490W, and ^{m}Y657W, respectively), and mutants ^{m}V687L, ^{m}K688R, ^{m}L684V and ^{m}S685T in the S3 pocket (M085-$I_{10\ \mu M}/I_{5\ \mu M}$ = 1.13 ± 0.26 and 1.80 ± 0.22 for ^{m}V687L and ^{m}K688R respectively; GSK1702934A-$I_{3\ \mu M}/I_{1\ \mu M}$ = 0.54 ± 0.07 and 1.39 ± 0.31 for ^{m}V687L and ^{m}K688R respectively) did not significantly alter the current ratio of M085 and GSK1702934A (Fig. 2, *D* and *E*; we could not assess the ratio change of ^{m}L684V and ^{m}S685T due to the loss of agonistic effect in these two mutations), suggesting that S1 and S3 are not important for the activation of mTRPC6 by M085 and GSK1702934A.

In contrast, we found that ^{m}E671C and ^{m}E672D, two mutants in S2, significantly altered the current ratios of M085 and GSK1702934A (M085-$I_{10\ \mu M}/I_{5\ \mu M}$ = 4.16 ± 0.87 and 3.27 ± 0.91 for ^{m}E671C and ^{m}E672D, respectively; GSK1702934A-$I_{3\ \mu M}/I_{1\ \mu M}$ = 6.10 ± 0.46 and 4.80 ± 1.23 for ^{m}E671C and ^{m}672D, respectively; Fig. 2, *D* and *E*), suggesting that these two structurally distinct small molecules may have the same mechanism of action. Combined with the observations of inside-out- and outside-out- macro-patch and site-directed mutagenesis, S2 is likely to be the key site for the activation of M085 and GSK1702934A in mTRPC6.

Dynamic interactions of M085 and GSK1702934A with the site formed by the pore helix and TM helix S6 of TRPC6

Before further delving into the mechanism of M085/GSK1702934A interaction with TRPC6, both unbiased (conventional molecular dynamics, CMD) and biased (metadynamics, MetaD) conformation sampling approaches were used to evaluate the interaction of S2 with these two compounds from a dynamic perspective, which can effectively improve the accuracy of mode derived from *in silico* docking.

MetaD, a method based on free-energy reconstruction and acceleration of rare events (30), has been used to study chemical reaction processes, protein–small molecule interactions (31), and optimal pathway for conformational changes in macromolecules (32–34), with the help of which the stretching of agonists (M085 and GSK1702934A) from the putative binding site and all binding modes between agonists and hTRPC6 can be evaluated extensively. During this process, the relative binding free energy for each binding mode could be measured simultaneously. MetaD simulations revealed the best binding modes for the interaction of M085 and GSK1702934A with hTRPC6 (Fig. 3, *A* and *B*). The optimal pose with low-binding free-energy exhibits almost the same interaction pattern of hTRPC6 and GSK1702934A as shown in the cryo-EM structure of hTRPC6 in complex with AM-0883: GSK1702934A is tightly locked by hydrogen bonding (H-bond) to the side chains of ^{h}W680 and ^{h}N702 (corresponding to ^{m}W679 and ^{m}N701 of mTRPC6, respectively) and cation-π interactions with ^{h}K698 and ^{h}F679 (identical to ^{m}K697 and

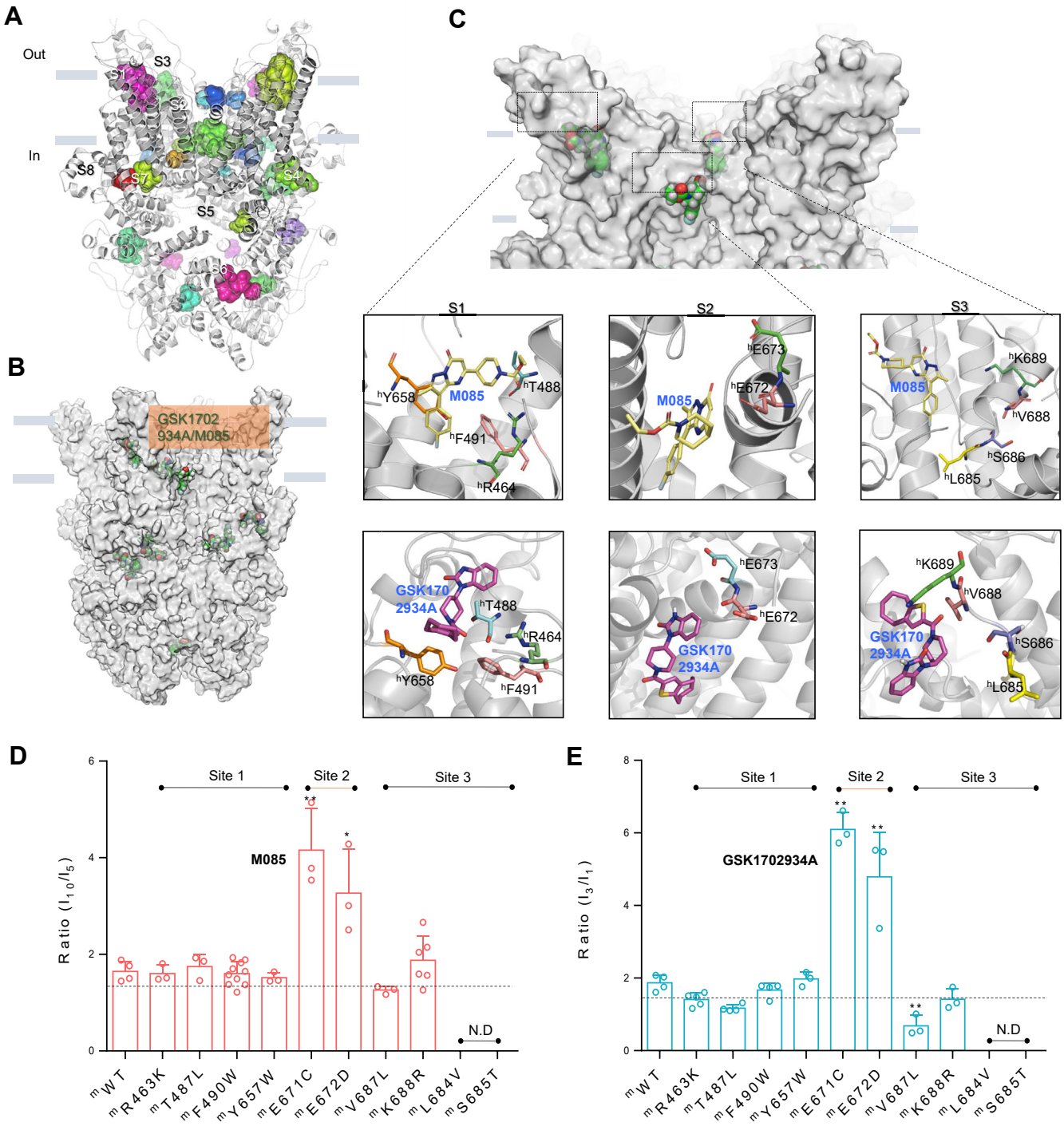

Figure 2. Possible interactions between M085/GSK1702934A and extracellular sites of TRPC6. *A*, three-dimensional (3D) structure of hTRPC6. S1 to S9 indicate nine potential sites that can bind small molecules. *B, in silico* docking of M085 and GSK1702934A into nine potential binding sites of hTRPC6. *C*, zoom-in view of contacts between M085/GSK1702934A and S1 to S3 extracellular sites in hTRPC6 (PDB ID: 5YX9; the missing loop was filled using the identical region of structure 6CUD). *D* and *E*, pool data showing ratio of currents mediated by different concentrations of M085 ($I_{10\ \mu M}/I_{5\ \mu M}$) and GSK1702934A ($I_{3\ \mu M}/I_{1\ \mu M}$) in mTRPC6-WT and its mutants. Data were presented as mean ± S.D. (n = 3–5). *$p < 0.05$; **$p < 0.01$ *versus* WT, one-way ANOVA with Bonferroni *post hoc* test ($F(8, 23) = 18.35$, $p < 0.001$) and ($F(8, 23) = 63.69$, $p < 0.0001$) for (*D*) and (*E*), respectively. ND, not determined.

^{m}F678 in mTRPC6, respectively; Fig. 3*A*). Almost the same interaction of M085 with site S2 was revealed by MetaD, where M085 is tightly locked by H-bond to the side chains of ^{h}W680 and ^{h}N702, and cation-π with ^{h}F675 (Fig. 3*B*).

We also further evaluated the rationality of above modes using CMD simulations. Protein–ligand interactions were monitored throughout the MD simulations and these interactions can be classified into four types: H-bonds,

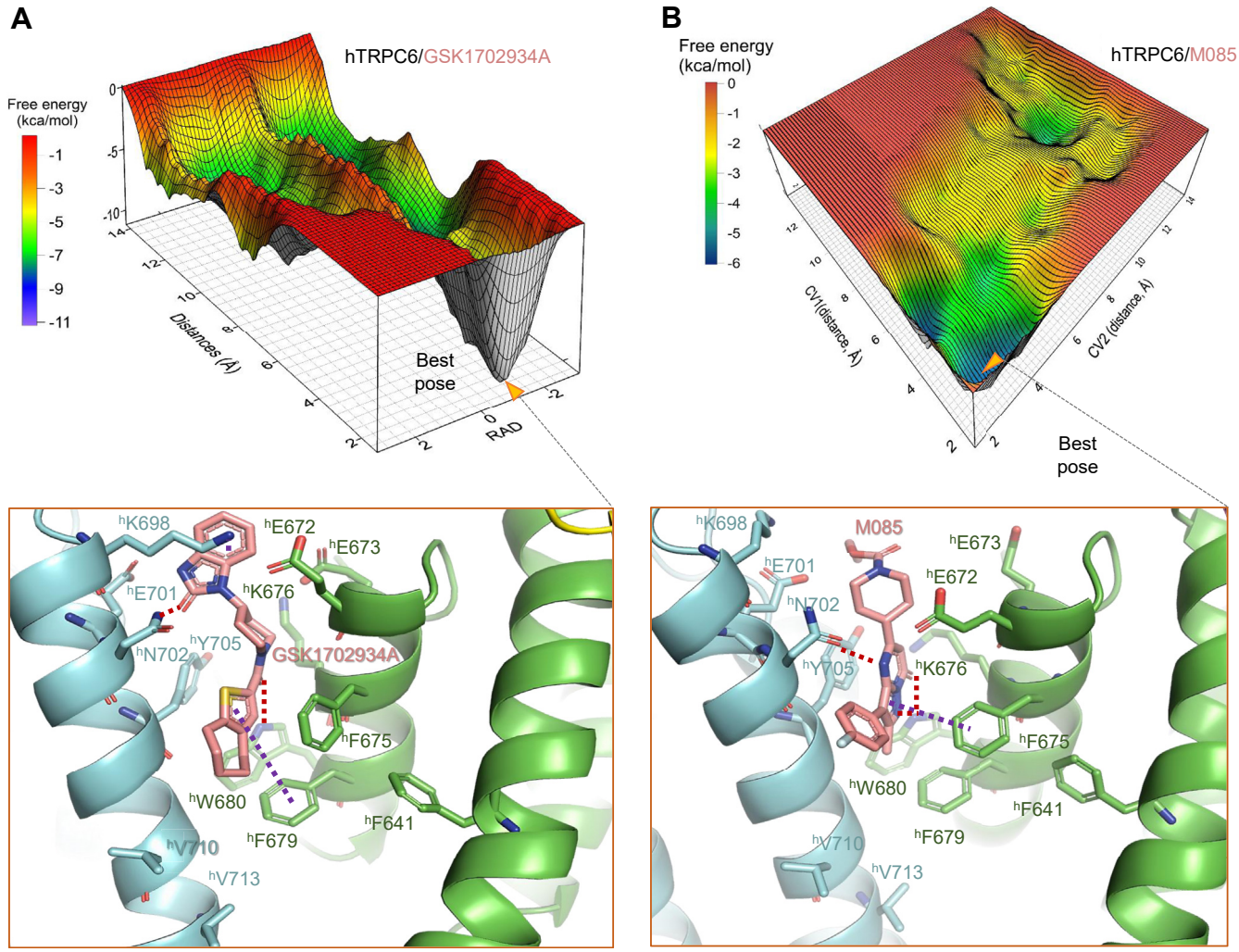

Figure 3. An optimization of interaction between hTRPC6 and GSK1702934A/M085 using metadynamics simulations. *A* and *B*, three-dimensional projection of the free-energy (kcal/mol) surface showing the pose with the lowest binding free-energy of GSK1702934A (*A*) and M085 (*B*) in hTRPC6. *Purple* and *red dotted lines* indicate Cation-π and H-bond contacts between GSK1702934A and hTRPC6, respectively.

hydrophobic, ionic, and water bridges (Fig. 4, *A* and *B*). A timeline representation of the interaction and contact of hTRPC6 with M085 and GSK1702934A was also summarized (Fig. 4, *C* and *D*). hTRPC6 interacting with GSK1702934A was very stable in CMD simulations, during which ^{h}F675, ^{h}F679, ^{h}W680, ^{h}N702, and ^{h}Y705 (corresponding to ^{m}F674, ^{m}F678, ^{m}W679, ^{m}N701, and ^{m}Y704 in mTRPC6, respectively) interacted with GSK1702934A *via* hydrophobic, H-bond, cation-π, or water-bridge contacts (Fig. 4, *B* and *D*). ^{h}E672, ^{h}F675, ^{h}W680, ^{h}E701, ^{h}N702, and ^{h}Y705 (corresponding to ^{m}E671, ^{m}F674, ^{m}W679, ^{m}E700, ^{m}N701, and ^{m}Y704 of mTRPC6) were also able to find similar interactions with M085 (Fig. 4, *A* and *C*). The ligand torsion diagram (Fig. 4, *E* and *F*) summarized the conformational evolution of each rotatable bond in the ligand throughout the simulated trajectory, where the two-dimensional schematic of the ligand was shown with color-coded rotatable bonds. The dial diagram and the bar diagram of the same color were shown for each twist of the rotatable bond. The dial (or radial) diagram depicted the conformation of the twist throughout the simulation. The start of the simulation was at the center of the radial plot, and the evolution of time was plotted radially outward. This analysis showed that agonist binding to TRPC6 was effective in limiting the conformational fluctuations of these two small molecules (except for the methoxy group of M085), especially for GSK1702934A, which may account for the better affinity of GSK1702934A compared with M085 (Fig. 4, *E* and *F*).

Mutations of residues in the orthosteric site significantly reduce the apparent affinity of M085/GSK1702934A

Compared with M085 activation of WT TRPC6 channels (EC_{50} = 3.80 ± 0.67 μM), ^{m}E671C, ^{m}E672D, ^{m}K675R, ^{m}N701Q, ^{m}Y704W, ^{m}K697R, and ^{m}V709A (EC_{50} = 23.32 ± 6.86, 25.06 ± 5.64, 6.90 ± 2.36, 55.71 ± 15.19, 26.67 ± 4.04, 14.12 ± 1.95 and 6.95 ± 2.13 μM for ^{m}E671C, ^{m}E672D, ^{m}K675R, ^{m}N701Q, ^{m}Y704W, ^{m}K697R, and ^{m}V709A corresponding to ^{h}E672C, ^{h}E673D, ^{h}K676R, ^{h}N702Q, ^{h}Y705W, ^{h}K698R, and ^{h}V710A of hTRPC6, respectively) significantly reduced the affinity of M085 and shifted the EC_{50} curve to the right. Similarly, compared with GSK1702934A activation of WT TRPC6 (EC_{50} = 0.78 ± 0.16 μM), ^{m}E671C, ^{m}E672D, ^{m}K675R, ^{m}N701Q,

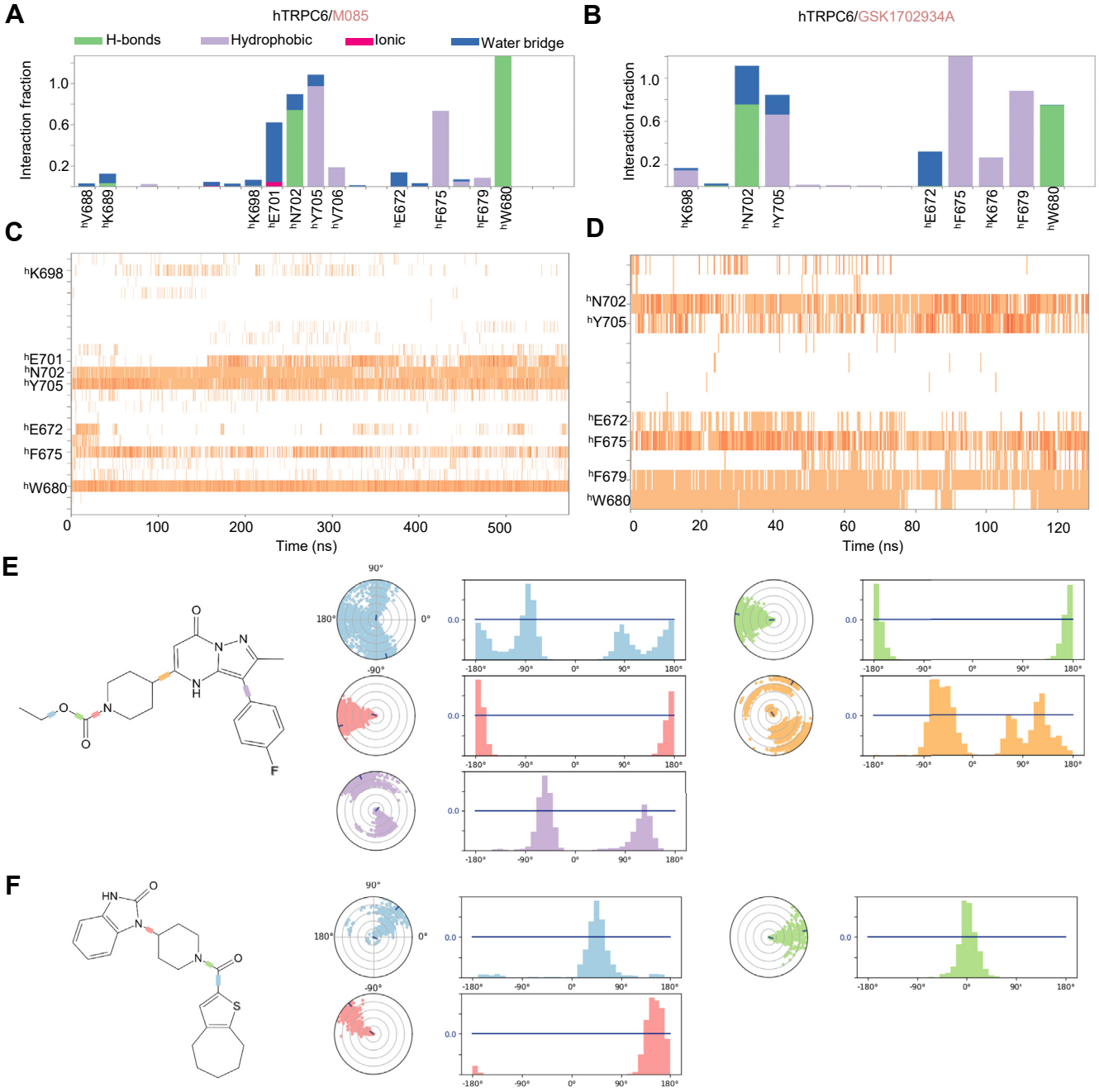

Figure 4. M085 and GSK1702934A produce stable contacts with ^{h}N702, ^{h}Y705, ^{h}F675, and ^{h}W680 during CMD simulations of hTRPC6. *A* and *B*, hTRPC6/M085 (*A*) and hTRPC6/GSK1702934A (*B*) interactions monitored throughout the simulations of hTRPC6-WT. *C* and *D*, timeline representations of hTRPC6/M085 (*C*) and hTRPC6/GSK1702934A (*D*) contacts. *E* and *F*, the M085 and GSK1702934A torsions plot summarization of the conformational evolution of every rotatable bond in M085 (*E*) and GSK1702934A (*F*) throughout the simulation trajectory. Each rotatable bond (color-coded) torsion is accompanied by a radial plot (*left*) and bar plots of the same color (*right*). The radial plot depicts the conformation of the torsion throughout the course of the simulation. The beginning of the simulation is in the center of the radial plot, and the time evolution is plotted radially outward. The bar plot summarizes the data on the radial plot, showing the probability density of the torsion. The histogram and torsion potential relationships give insights into the conformational strain the ligand undergoes to maintain a protein-bound conformation.

^{m}Y704W, ^{m}K697R, and ^{m}V709A (EC_{50} = 6.63 ± 0.40, 1.80 ± 0.33, 4.76 ± 0.41, 5.37 ± 0.30, 2.93 ± 0.74, 1.19 ± 0.14, and 2.61 ± 0.26 μM, respectively) also remarkably reduced the GSK1702934A apparent affinity and right shifted the concentration–response curve. Meanwhile, we found that mutant ^{m}F640W (corresponding to ^{h}F641W) had the effect of enhancing the apparent affinity of M085 (EC_{50} = 0.84 ± 0.27 μM) and GSK1702934A (EC_{50} = 0.27 ± 0.05 μM) and shifted the EC_{50} curve to the left ($p < 0.01$, n = 3–4) (Fig. 5*B*). Thus, the subunit interface between the PH and S6 might be the orthosteric site responsible for both M085 and GSK1702934A-mediated channel activations.

Additionally, these important residues in hTRPC6 (M085-EC_{50} = 50.16 ± 6.65, 22.13 ± 5.46, 44.00 ± 5.75, 54.50 ± 6.53, and 35.30 ± 6.15 μM for ^{h}E672C, ^{h}E673D, ^{h}K676R, ^{h}N702Q, and ^{h}Y705W, respectively; GSK1702934A-EC_{50} = 4.47 ± 0.37,

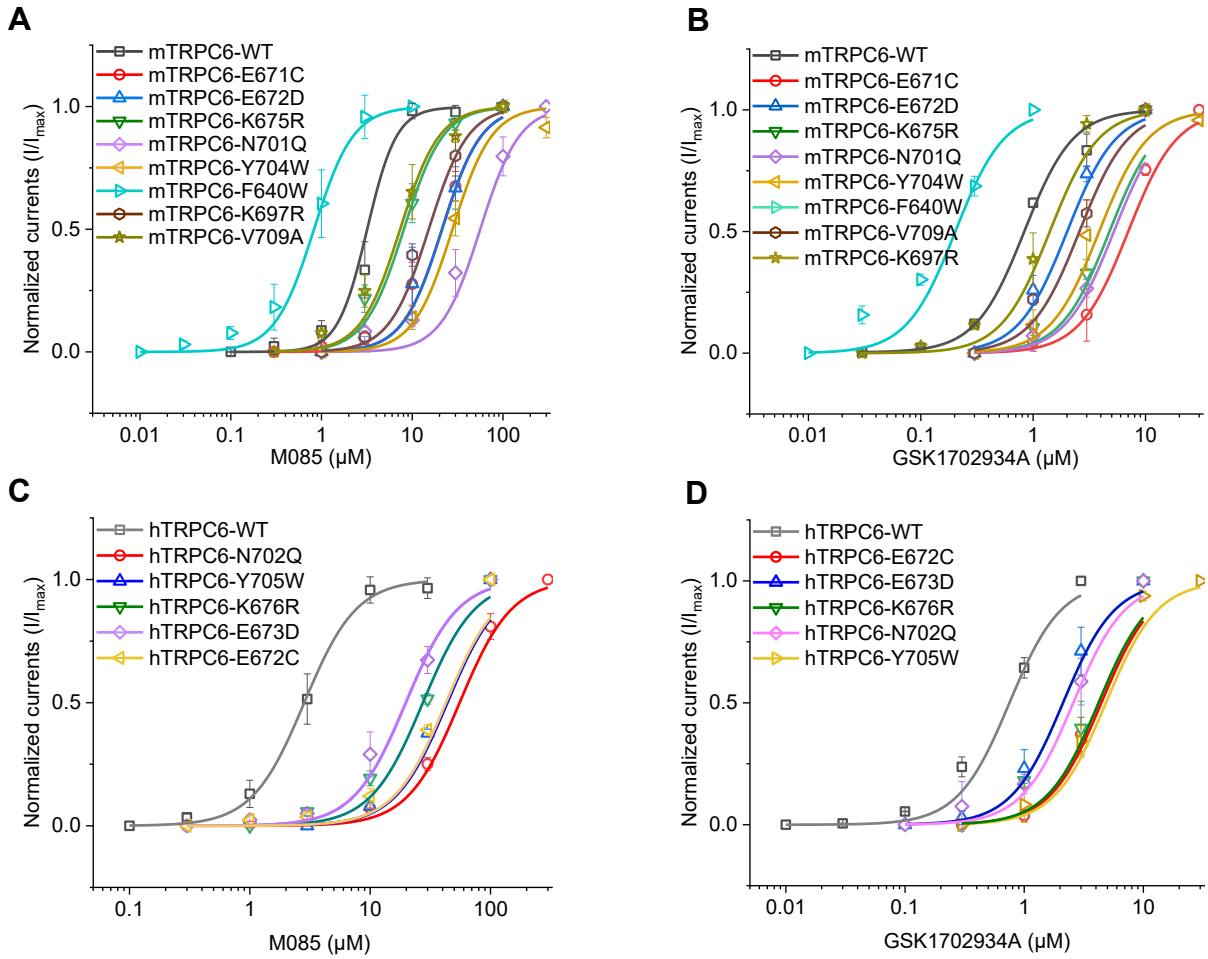

Figure 5. Single amino acid substitutions at the orthosteric site formed by the pore helix and S6 significantly reduce the apparent affinity of M085/GSK1702934A. *A* and *B*, concentration–activation curves of mTRPC6-WT and its mutants induced by M085 (*A*) and GSK1702934A (*B*). *C* and *D*, concentration–activation curves of hTRPC6-WT and its mutants induced by M085 (*C*) and GSK1702934A (*D*). Data points were presented as mean ± S.D. (n = 3–4) and fitted with Hill equation.

2.04 ± 0.60, 4.08 ± 1.04, 3.07 ± 0.81, and 3.92 ± 0.37 μM for ^{h}E672C, ^{h}E673D, ^{h}K676R, ^{h}N702Q, and ^{h}Y705W, respectively) were also found to be significantly reduced in the apparent affinity of M085/GSK1702934A compared with WT hTRPC6 channels (EC_{50} = 2.94 ± 0.70 and 0.45 ± 0.03 μM for M085/GSK1702934A in hTRPC6, respectively; Fig. 5, *C* and *D*), which is consistent with mTRPC6. Therefore, it should be reasonable that all mutagenesis, electrophysiological recordings, and protein surface expression analysis were performed on mTRPC6, while *in silico* docking, MetaD and CMD simulations were carried out in the cryo-EM structures of hTRPC6.

Mutations of residues in the orthosteric site do not alter the surface expression of mTRPC6 but significantly reduce the maximal agonistic effect and alter the channel gating of M085 and GSK1702934A

Compared with WT mTRPC6 currents induced by saturated M085 (I_{max} = 75.11 ± 14.20 pA/pF, 30 μM M085) and GSK1702934A (I_{max} = 95.64 ± 14.62 pA/pF, 10 μM GSK1702934A), ^{m}E671C, ^{m}E672D, ^{m}K675R, ^{m}N701Q, ^{m}Y704W, and ^{m}K697R significantly decreased maximal currents of these two agonists (M085-I_{max} = 24.09 ± 4.53, 10.28 ± 1.19, 8.26 ± 0.62, 2.11 ± 1.04, 3.27 ± 1.12, and 25.58 ± 1.86 pA/pF for ^{m}E671C, ^{m}E672D, ^{m}K675R, ^{m}N701Q, ^{m}Y704W, and ^{m}K697R, respectively, 100 μM M085; GSK1702934A-I_{max} = 27.38 ± 4.69, 11.72 ± 1.02, 1.43 ± 0.20, 0.86 ± 0.59, 6.88 ± 2.31, and 8.53 ± 2.36 pA/pF for ^{m}E671C, ^{m}E672D, ^{m}K675R, ^{m}N701Q, ^{m}Y704W, and ^{m}K697R respectively, 100 μM GSK1702934A; Fig. 6, *A* and *B*), indicating that amino acids at the interface of the PH and S6 helix are important for the function of mTRPC6, and any change in their charge or size of these residues may lead to abnormalities in the function of mTRPC6. In addition, small changes in side chain size of two residues, ^{m}F678W and ^{m}W679F, had caused complete loss of function in mTRPC6 (Fig. 6*A*). To further illustrate this point, we also added alanine-substitution mutants to residues located in PH and S6 that interact strongly with GSK1702934A or M085 (Fig. 4, *A–D*), *i.e.*, ^{m}F674A, ^{m}W679A, ^{m}E700A, ^{m}N701A, and ^{m}Y704A (corresponding to ^{h}F675A, ^{h}W680A, ^{h}E701A, ^{h}N702A, and ^{h}Y705A) (Figs. 3 and 4, *A–D*), all of which resulted in the disappearance of GSK1702934A/M085 current (Fig. 6*A*).

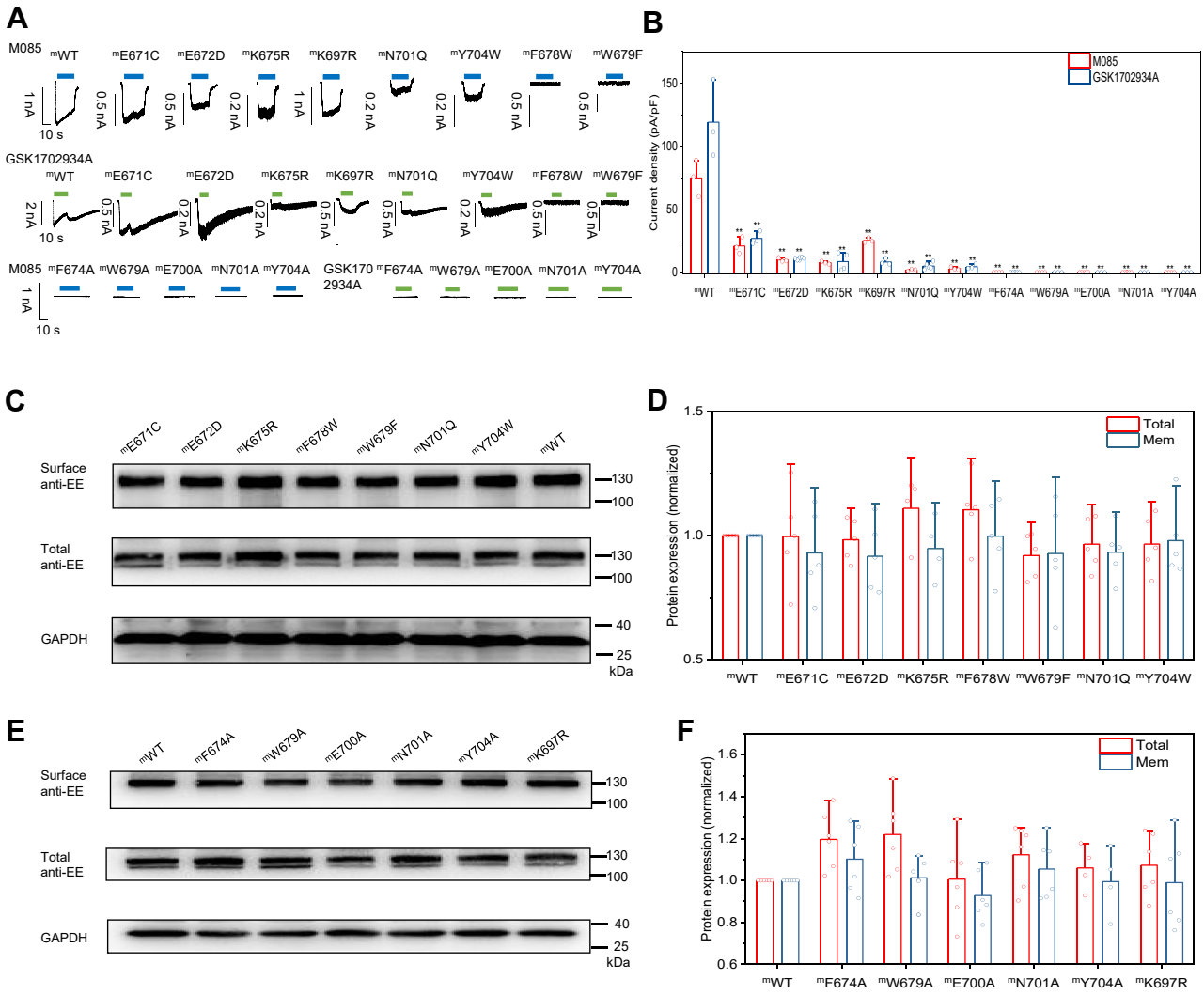

Figure 6. Single residue replacements at the orthosteric site do not alter the membrane expression of mTRPC6, but significantly reduce the maximum agonistic effect of M085 and GSK1702934A. *A* and *B*, representative current traces (*A*) and pooled data (*B*) of mTRPC6-WT and its mutants induced by saturated M085 and GSK1702934A. All data are expressed as mean ± S.D. Each mutant was repeated at least three times for independent experiments. $^{**}p < 0.01$ *versus* WT, one-way ANOVA with Bonferroni *post hoc* test ($F(11, 31) = 87.89$, $p < 0.0001$) and ($F(11, 31) = 49.88$, $p < 0.0001$) for M085 and GSK1702934A, respectively. *C* and *D*, representative Western blotting (*C*) and mean values (*D*) of the membrane and total expressions of mTRPC6-WT and its mutants. At least four experiments were performed for WT and each mutant. $^{*}p < 0.05$, $^{**}p < 0.01$ *versus* WT, one-way ANOVA with Bonferroni *post hoc* test ($F(7, 31) = 1.490$, $p = 0.2075$) and ($F(7, 31) = 0.2690$, $p = 0.9614$) for total and surface expressions, respectively. *E* and *F*, representative Western blots (*E*) and means (*F*) of membrane and total expression of mTRPC6-WT and mutants in which alanine substitutions on key residues produced strong contacts with M085 and GSK1702934A during MD simulations. At least four experiments were performed for WT and each mutant. $^{*}p < 0.05$, $^{**}p < 0.01$ *versus* WT, one-way ANOVA with Bonferroni *post hoc* test ($F(6, 33) = 2.122$, $p = 0.0771$) and ($F(6, 33) = 0.9172$, $p = 0.4951$) for total and surface expressions, respectively.

To examine whether the reduction in the maximum current of agonist response of key residues might be due to altered protein surface expression, the surface biotinylation and Western blotting were used to determine the surface and total protein levels. The protein surface expression levels of ^{m}E671C, ^{m}E672D, ^{m}K675R, ^{m}F678W, ^{m}W679F, ^{m}N701Q, ^{m}Y704W, ^{m}K697R, ^{m}F674A, ^{m}W679A, ^{m}E700A, ^{m}N701A, and ^{m}Y704A were comparable to that of WT ^{m}TRPC6 (Fig. 6, *C–F*), suggesting that these substitutions reduced the agonistic potency of M085 and GSK1702934A in mTRPC6 perhaps through altered channel gating rather than reduced receptor expression. In particular, the side chain of ^{m}W679 formed H-bond contacts with M085 and GSK1702934A, which is essential for their bindings (Fig. 3), but we could not assess EC_{50} changes because mutations at this site resulted in a loss of agonistic effect. Normal surface expression of ^{m}W679F and ^{m}W679A (Fig. 6, *C–F*) demonstrated that the loss of function of this mutant (Fig. 6, *A* and *B*) is caused more by altering conformation required for the agonist recognition and/or channel gating of TRPC6. Similar results could also be observed in ^{m}F674A, ^{m}E700A, ^{m}N701A, and ^{m}Y704A (Fig. 6, *A*, *B*, *E* and *F*). These results suggest that the key amino acids predicted by *in silico* docking, MetaD and MD simulations are important recognition residues for M085 and GSK1702934A.

Unitary currents of M085 and GSK1702934A were recorded in an outside-out configuration in HEK293 cells expressing mTRPC6. At −60 mV clamp voltage, both M085 (100 μM) and GSK1702934A (1 μM) induced full channel opening with a

unitary current of approximate 2.2 pA (Fig. 7, *A–D*) and a conductance of ∼35 pS, the value consistent with previous studies (25, 35). Interestingly, in the presence of saturated GSK1702934A (100 μM) and M085 (100 μM), the unit current of mTRPC6^{N701Q} reached only about 1.1 pA at −60 mV, and most of the channels were closed or in sub-open states (Fig. 7, *E–H*). In addition, we did not record unit currents for GSK1702934A (100 μM) and M085 (100 μM) in mTRPC6^{W679F} (Fig. 7, *I–L*), despite normal surface expression of this mutant in HEK-293 cells (Fig. 6, *C* and *D*). These results suggest that ^{m}N701Q and ^{m}W679F significantly impaired GSK1702934A- and M085-induced gating of mTRPC6.

Occupancy of the orthosteric site via *covalent modification on ^{m}E671C abolishes M085/GSK1702934A-mediated TRPC6 activation*

To further explore the critical role of the putative subunit interface between the S6 and PH in agonist recognition, we replaced ^{m}E671 with cysteine with the aim of impairing M085/GSK1702934A binding by covalently occupying this orthosteric site. 5,5′-dithiobis (2-nitrobenzoic acid) (DTNB) is used here to study the effect of covalent occupancy of the binding site, whose thiobenzene (2-nitrobenzoic acid) (TNB) moiety could be covalently attached to free cysteine *via* a disulfide bond (36, 37) (Fig. 8*A*). For WT TRPC6 channels, DTNB had no effect on GSK1702934A- and M085-mediated activations of mTRPC6 (Fig. 8*C*), which is consistent with the lack of distribution of free cysteine residues in the extracellular region of the natural receptor.

As mentioned above (Fig. 5, *A* and *B*), the ^{m}E671C mutant reduced the affinity of M085/GSK1702934A and shifted the concentration–response curve to the right (Fig. 8*B*), indicating its important role in the orthosteric site. Interestingly, M085- or GSK1702934A-mediated activation in mTRPC6^{E671C} was completely inhibited after DTNB (2 mM)-treatment, and application of dithiothreitol (DTT, 10 mM) to remove the TNB moiety from the receptor partially "recovered" the current of M085/GSK1702934A (Fig. 8, *C* and *D*), suggesting that the specific covalent modification on ^{m}E671C may interrupt the recognition of the ligand. Thus, the putative subunit interface between S6 and PH is involved in the recognition of M085 and GSK1702934A.

Discussion

In this study, we demonstrate that two structurally distinct TRPC6 agonists, M085 and GSK1702934A, both act at an extracellular site formed by PH and S6, which might be the only orthosteric site that can accept extracellular small-molecule agonists during TRPC6 sequence evolution. We used both outside- and inside-out electrophysiological recording patterns to demonstrate that the binding site for M085 and GSK1702934A exists extracellularly rather than intracellularly (Fig. 1, *E* and *F*). When M085 (or GSK1702934A) was *in silico* docked to hTRPC6, three potential extracellular binding pockets (S1, S2, and S3) were identified, and mutation screening revealed that two of them (S1 and S3) were not the binding pockets of M085 and GSK1702934A, while S2 was most likely the binding pocket of GSK1702934A and M085 (Fig. 2, *D* and *E*). We further evaluated the rationality and stability of the interaction of TRPC6 with these two compounds in the S2 pocket by combining CMD and MetaD simulations (Figs. 3 and 4). Meanwhile, mutations of amino acids in the S2 pocket could significantly reduce the apparent affinity of M085/GSK1702934A (Fig. 5). The reduced agonistic effect was not caused by a reduction in the membrane expression of TRPC6 (Fig. 6, *C–F*). In addition, mutations of residues in the orthosteric site reduced the channel opening probability and conductance of mTRPC6 (Fig. 7, *E–L*). After DTNB's covalent occupancy in ^{m}E671C, currents of M085 and GSK1702934A were completely suppressed and were partially restored after DTT reduction (Fig. 8*C*). All these data suggest that the site formed by PH and S6 is critical for the extracellular activation of M085 and GSK1702934A.

Our results also coincide with some observations from other TRP subfamilies or with corresponding sites in other TRPC subtypes. For example, previous studies have identified a similar site near the subunit interface between the S6 and PH, which has been identified as a binding site for the agonist of TRPML1 (ML-SA1) (38). Meanwhile, studies of TRPC5 have identified this region as the binding site for both the endogenous lipid and the exogenous inhibitor Pico145 (39). In TRPC4, it has been shown that the phosphate head group of phospholipids (PA) interacts with main chain atom and side chains of T599 (in the S6 helix), W573 and Q569 (in the pore helix). In addition, DAG activation of TRPC6 is likely to stimulate at the lipid-binding site close to the pore region of the channel and therefore promotes channel opening (40). Recent structural analysis of the open state of TRPC6 has also shown that the small-molecule AM-0883 can bind to this site as well (28).

Three structurally distinct agonists, M085, GSK1702934A, and AM-0883 (10, 28), all act on this binding pocket, implying that this site may be the only orthosteric site that could recognize extracellular small-molecule agonists during evolution of TRPC sequences. Certainly, we cannot exclude the possibility that large-molecular-weight toxins act on the large extracellular domain of TRPC6 and thus lead to channel activation. For example, the agonist of TRPV1, double junctional toxin DkTx, binds to the extracellular domain of the TRPV1 channel. Its two junctions bind at two equivalent positions on two adjacent subunits of this tetrameric channel, straddling between the two subunits, while DkTx 's junctions are connected by a segment of the liner that keeps the TRPV1 channel in the open state (41). In contrast, from the perspective that small molecules are limited in size and can only bind in restricted regions, this site formed by PH and S6 may be the only orthosteric site for TRPC6 to be activated by extracellular small molecules.

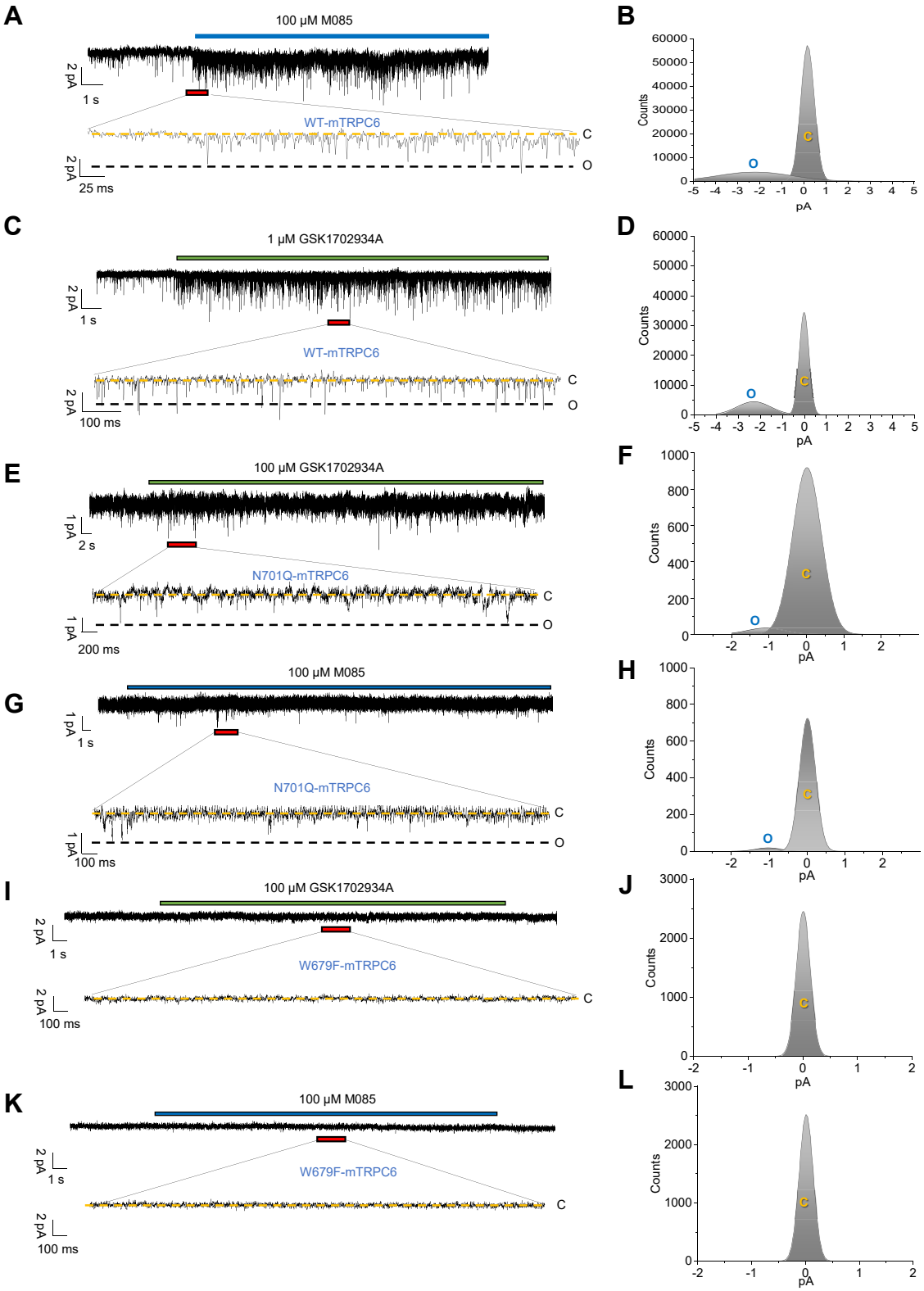

Figure 7. Mutations of the orthosteric site alter the unitary current of TRPC6 induced by M085 and GSK1702934A. *A–D*, unitary currents recorded from outside-out patches held at −60 mV in responses to 100 μM M085 (*A* and *B*) and 1 μM GSK1702934A (*C* and *D*) for mTRPC6-WT. *E–H*, unitary currents recorded from outside-out patches held at −60 mV in responses to 100 μM GSK1702934A (*E* and *F*) and 100 μM M085 (*G* and *H*) for the ^{m}N701Q. *I–L*, unitary currents recorded from outside-out patches held at −60 mV in responses to 100 μM GSK1702934A (*I* and *J*) and 100 μM M085 (*K* and *L*) for the ^{m}W679F. Full opening (O) and closing (C) are indicated by *black* and *yellow lines*, respectively. y axis (count) denotes the ratio of the number of events to the number of bins (the bin number is set to 320). All results were repeated at least three times.

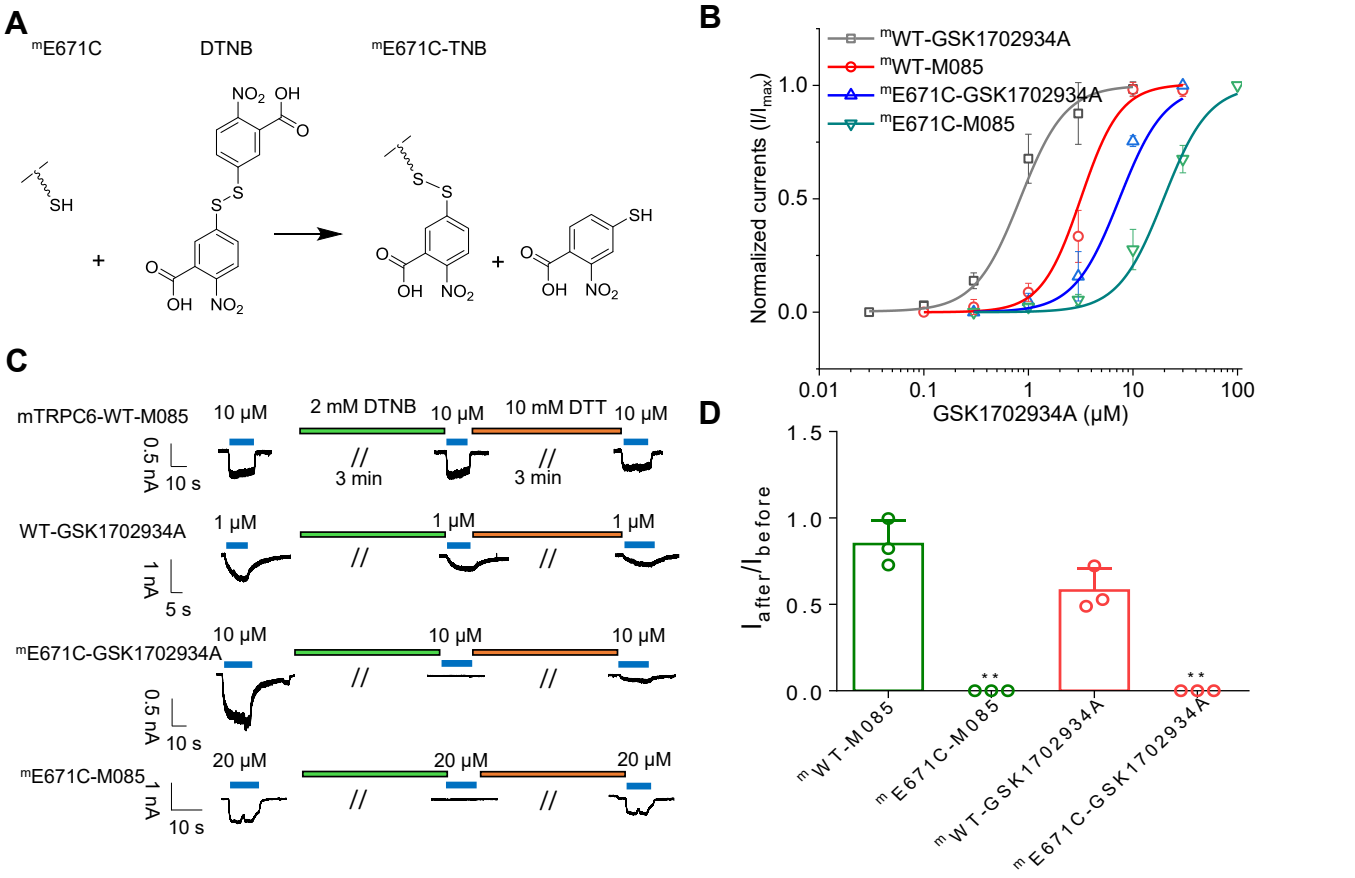

Figure 8. Covalent occupancy of the orthosteric site abolishes M085 and GSK1702934A-mediated TRPC6 activation. *A*, an illustration of the DTNB covalent-linking with cysteine (Ellman's reaction) on ^{m}E671C. *B*, concentration–activation curves of M085 and GSK1702934A in ^{m}E671C before and after DTNB modification. Data points were presented as mean ± S.D. (n = 3–4) and fitted with Hill equation. *C*, representative traces showing effects of DTNB's covalent modification on M085-and GSK1702934A-induced currents in ^{m}E671C and mTRPC6-WT. The reduced current after modification could be partially rescued by following DTT treatments, respectively. *D*, quantitative analysis and significance tests on M085-and GSK1702934A-induced currents of ^{m}E671C and mTRPC6-WT channels before and after modification by DTNB, respectively. $^{**}p < 0.01$ *versus* WT, student's *t* test.

The gating process of TRPC channels became clearer after structural determinations of different subtypes of the TRPC subfamily (42–44). hTRPC6's open structure in complex with AM-0883 revealed the mechanism of TRPC6 channel activation by AM-0883 (28), while AM-0883, M085, and GSK1702934A act at almost the same position, we infer that the gating mechanism of M085 and GSK1702934A activating TRPC6 is similar to that of AM-0883. During the gating of TRPC6, the binding of agonists (M085 and GSK1702934A) could not only cause structural rearrangement of the agonist binding pocket, but also push the extracellular region of S6 away from the pore and push S6 helix to the cytoplasmic side. Since S6 surrounds to S1 to S4 from the adjacent subunit, the movement of S6 is accompanied by the simultaneous tilting and downward movement of S1 to S4 as well as S4 to S5 linkers. From the cytoplasmic side, agonist binding is accompanied by a counterclockwise rotation around the central ion-permeable pathway, which eventually moves the intracellular portion of S1 to S4 a certain distance and opens the pore channel.

Taken together, this study not only advances our understanding of the contribution of PH and S6 to TRPC6 activation by providing a model to explain how the widely used agonists M085 and GSK1702934A bind to the receptor, but also reveals that this region might be the only extracellular small molecule agonist recognition site in TRPC. Notably, the sequences of the PH and S6 in TRPC3/6/7 are highly conserved, which poses a challenge for the development of TRPC3/6/7-specific small molecules. Our study will also be able to evaluate strategies to regulate TRPC function by stimulating the pocket formed between PH and S6 using new small molecules.

Experimental procedures

Drugs, cell culture, and mutagenesis

M085 and GSK1702934A were synthesized in our laboratory (see below). The plasmids for mTRPC6 and hTRPC6 were a gift from Xi Zhu. Each mutant was constructed by the KOD-Plus-Mutation Kit (Toyobo). Individual mutants were verified by DNA sequencing and then expressed in HEK293 cells. HEK293 cells were cultured in DMEM medium containing

10% fetal bovine serum, 1% penicillin/streptomycin, and 1% glutamine at 37 °C with 5% CO_2 and 95% air. Transfection of TRPC6 plasmids was performed with Hilymax (Dojindo Laboratories) according to the manufacturer's protocol. Electrophysiological measurements were performed 24 to 48 h after transfection on HEK293 cells.

Chemical synthesis of GSK1702934A

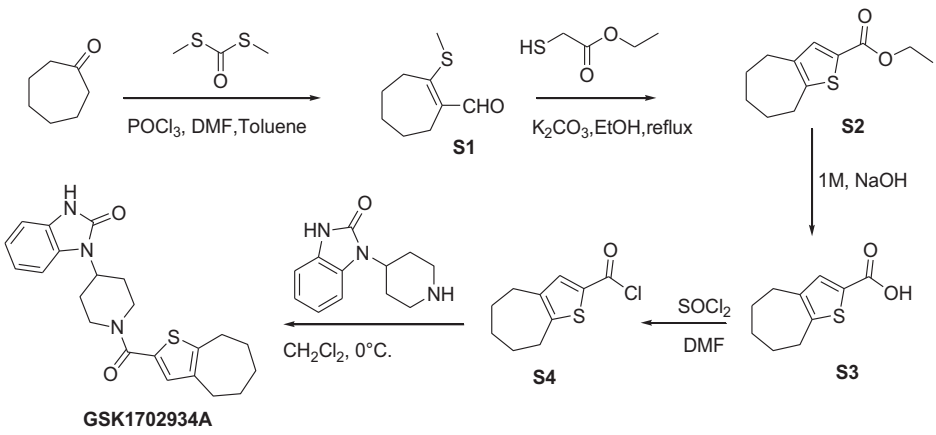

GSK1702934A was prepared according to previous descriptions (12, 45, 46). Briefly, to a solution of dimethyl formamide (DMF, 30 mmol) in dry toluene (30 ml), $POCl_3$ (30 mmol) was added at room temperature with stirring for 30 min, followed by addition of cycloheptanone (20 mmol) in toluene and further stirred for 3 h (monitored by TLC). The reaction mixture was then cooled in an ice bath, followed by addition of the dimethyldithiocarbonate (DDC, 20 mmol) and 30% aqueous KOH (20 ml) until the solution becomes basic. The solution was then heated at 90 °C for 45 min (monitored by TLC), cooled to room temperature and extracted with petroleum ether, and washed with water until the washings were neutral to litmus. The combined extracts were dried (Na_2SO_4), and the solvent was evaporated under reduced pressure to give crude product **S1** ((Z)-2-(methylthio)cyclohept-1-enecarbaldehyde), which was used for next reaction without purification.

To a solution of S1 (1.99 g, 11.7 mmol) in ethanol 50 ml was added ethyl thioglycolate (1.41 g, 11.7 mmol) and anhydrous potassium carbonate (1.62 g, 11.7 mmol) at room temperature. The mixture was heated to reflux for 1 h (monitored by TLC), then was cooled to room temperature, and evaporated the solvent. The residue was added with water and extracted with ethyl acetate. The combined extracts were dried (Na_2SO_4), and the solvent was evaporated under reduced pressure. The crude product was purified by column chromatography over silica gel using ethyl acetate-petroleum ether (5:95) as eluents. The compound S2 (ethyl 5,6,7,8-tetrahydro-4H-cyclohepta [b] thiophene-2-carboxylate) was obtained in 71% yield (1.85 g, 8.3 mmol). ^{1}H NMR (400 MHz, Chloroform-d) δ 7.47 (s, 1H), 4.31 (q, J = 7.1 Hz, 2H), 2.87 to 2.79 (m, 2H), 2.74 to 2.65 (m, 2H), 1.87 (qd, J = 5.9, 5.0, 1.8 Hz, 2H), 1.74 to 1.67 (m, 2H), 1.67 to 1.59 (m, 2H), 1.36 (t, J = 7.1 Hz, 3H).

A solution of **S2** (0.78 g, 3.5 mmol) in EtOH (30 ml) was treated with a solution of NaOH (1 M in water, 7 ml) and stirred at 85 °C for 1 h. The mixture was cooled to room temperature and acidified with 1 M HCl (30 ml). The resulting precipitate was filtered and washed with petroleum ether. The **S3** (5,6,7,8-tetrahydro-4H-cyclohepta[b]thiophene-2-carboxylic acid) was obtained as white solid (0.61 g, 89%). To a solution of S3 (0.35 g, 1.8 mmol) in $SOCl_2$ (15 ml) was added DMF 2 drops. The mixture was heated to reflux for 1 h, then cooled to room temperature, and evaporated under vacuum to afford quantitatively corresponding acid chloride **S4**.

To a mixture of 4-(2-keto-1-benzimidazolinyl)piperidine (0.39 g, 1.8 mmol) and trimethylamine (0.25 ml, 1.8 mmol) in CH_2Cl_2 (15 ml) added **S4** (in CH_2Cl_2 5 ml) by dropwise in an ice bath and stirred for 6 h (monitored by TLC). After completion of reaction, the mixture was washed thoroughly with brine. The organic layer was dried over anhydrous Na_2SO_4 and then concentrated to give crude product of GSK1702934A under reduced pressure. The residue was purified by silica gel chromatography to give the desired product (0.56 g, 79%) as a white solid.

^{1}H NMR (400 MHz, DMSO-d_6) δ 10.91 (s, 1H), 7.33 to 7.09 (m, 2H), 6.99 (dd, *J* = 6.0, 3.6 Hz, 3H), 4.48 (ddq, *J* = 12.4, 8.2, 4.0 Hz, 3H), 3.09 (q, *J* = 11.1, 7.9 Hz, 2H), 2.83 to 2.70 (m, 2H), 2.70 to 2.58 (m, 2H), 2.32 (qd, *J* = 12.5, 4.1 Hz, 2H), 1.79 (td, *J* = 10.3, 9.0, 5.0 Hz, 4H), 1.57 (dp, *J* = 21.7, 5.0 Hz, 4H).

Chemical synthesis of M085

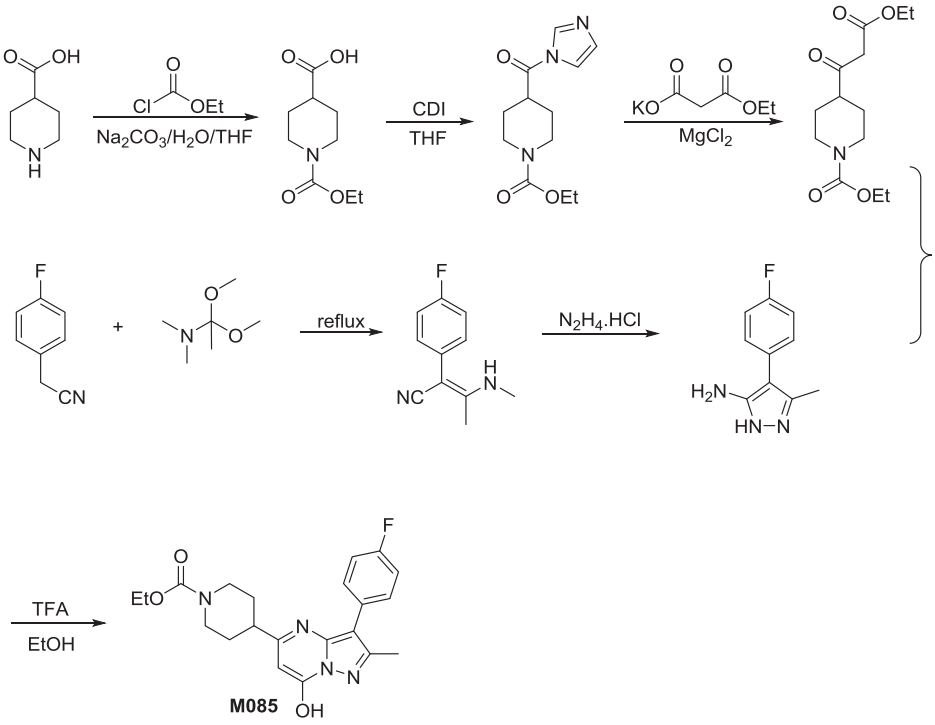

Ethyl 4-(3-ethoxy-3-oxopropanoyl)piperidine-1-carboxylate

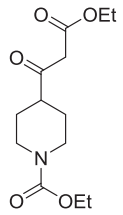

To a solution of piperidine-4-carboxylic acid (2.58 g, 20 mmol) in water (20 ml) was added Na_2CO_3 (2.52 g, 24 mmol), and then was added ethyl chloroformate (2.56 g, 24 mmol) in THF (20 ml). The reaction mixture was stirred at room temperature until completion and then concentrated *in vacuo*. Water (30 ml) was added into the mixture and then was adjusted to pH 2 using 2 M HCl. The aqueous layer was extracted with EtOAc (3 × 15 ml). The combined organic layers were washed with brine, dried over anhydrous Na_2SO_4, filtered, and concentrated *in vacuo*.

The residue dissolved in THF (8 ml) was added N, N′-carbonyldiimidazole (4.21 g, 26 mmol). The reaction mixture was stirred at room temperature until completion and then concentrated *in vacuo*.

To a solution of ethyl potassium malonate (6.8 g, 40 mmol) in THF (100 ml)/CH_3CN (50 ml) was added anhydrous $MgCl_2$ (3.8 g, 40 mmol) and DMAP (244 mg, 2 mmol) at 0 °C. The above residue dissolved in THF (10 ml) was added into the mixture, and then was added Et_3N (3.03 g, 40 mmol). The reaction mixture was stirred at room temperature until completion, and then was added 1 M HCl (150 ml). The aqueous layer was extracted with Et_2O (3 × 100 ml). The combined organic layers were washed with brine, dried over anhydrous Na_2SO_4, filtered, and concentrated *in vacuo*. The residue was purified by flash chromatography to give the yellow oil (4.39 g, 81% for three steps).

^{1}H NMR (300 MHz, $CDCl_3$) δ 4.27 to 4.03 (m, 5H), 3.48 (s, 1H), 3.38 (s, 1H), 2.84 (t, J = 11.5 Hz, 1H), 2.67 to 2.59 (m, 1H), 2.07 (s, 1H), 1.85 (d, J = 11.9 Hz, 1H), 1.61 to 1.49 (m, 1H), 1.29 to 1.21 (m, 6H). ESI-MS *m/z* 272.1 $[M + H]^+$.

4-(4-Fluorophenyl)-3-methyl-1H-pyrazol-5-amine

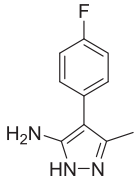

To a solution of 4-fluorophenylacetonitrile (0.65 g, 4.8 mmol) in DMF (5 ml) was added 1,1-dimethoxy-N,N-dimethylethylamine (0.53 g, 4 mmol). The reaction mixture was stirred at 100 °C until completion and then concentrated *in vacuo*. Hydrazine monohydrochloride (0.41 g, 6 mmol), EtOH (8 ml) and

water (5 ml) were added into the reaction mixture and then stirred at 80 °C until completion. Saturated $NaHCO_3$ solution (30 ml) was added, and the aqueous layer was extracted with EtOAc (3 × 10 ml). The combined organic layers were washed with brine, dried over anhydrous Na_2SO_4, filtered, and concentrated *in vacuo*. The residue was recrystallized with PE/EtOAc to give a white solid (0.82 g, 90% for two steps).

^{1}H NMR (500 MHz, DMSO-d_6) δ 7.38 (dd, *J* = 8.6, 5.7 Hz, 2H), 7.21 (t, *J* = 8.9 Hz, 2H), 2.17 (s, 3H). ESI-MS *m/z* 192.1 $[M + H]^+$.

3-Methyl-4-(4-(trifluoromethyl)phenyl)-1H-pyrazol-5-amine

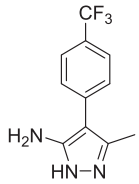

Following the prepare procedure of 4-(4-fluorophenyl)-3-methyl-1H-pyrazol-5-amine, 3-methyl-4-(4-(trifluoromethyl) phenyl)-1H-pyrazol-5-amine was prepared from 4-trifluoromethylphenylacetonitrile as a white solid in 88% yield.

^{1}H NMR (500 MHz, DMSO-d_6) δ 7.82 (d, *J* = 8.0 Hz, 2H), 7.64 (t, *J* = 8.4 Hz, 2H), 2.31 (s, 3H). ESI-MS *m/z* 242.1 $[M + H]^+$.

Ethyl 4-(3-(4-fluorophenyl)-7-hydroxy-2-methylpyrazolo[1,5-a] pyrimidin-5-yl)piperidine-1-carboxylate (M085)

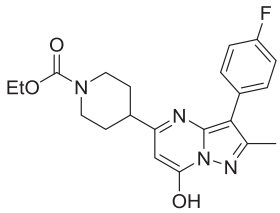

To a solution of 4-(4-fluorophenyl)-3-methyl-1H-pyrazol-5-amine (3.82 g, 20 mmol) in AcOH (20 ml) was added ethyl 4-(3-ethoxy-3-oxopropanoyl) piperidine-1-carboxylate (7.99 g, 24 mmol). The reaction mixture was stirred at 130 °C until completion and then concentrated *in vacuo*. 1 M NaOH was added into the mixture and filtered to give a white solid (6 g, 75% yield).

^{1}H NMR (500 MHz, DMSO-d_6) δ 7.91 (dd, *J* = 8.6, 5.8 Hz, 2H), 7.21 (t, *J* = 8.9 Hz, 2H), 5.46 (s, 1H), 4.18 to 4.00 (m, 4H), 2.90 (brs, 2H), 2.65 to 2.57 (m, 1H), 2.50 (s, 3H), 1.87 to 1.84 (m, 2H), 1.65 to 1.59 (m, 2H), 1.25 to 1.19 (m, 3H). ^{13}C NMR (125 MHz, DMSO-d_6) δ 165.4, 160.1, 158.4, 158.2, 154.6, 148.9, 147.2, 131.7, 128.4, 128.4, 114.6, 114.4, 101.8, 90.0, 60.5, 43.7, 43.4, 31.1, 15.0, 14.5. ESI-MS *m/z* 421.3 $[M + Na]^+$.

In silico *docking*

The cryo-EM structure of hTRPC6 (PDB 5YX9) was prepared using the Protein Preparation Wizard (47) after filling the missing loop using Modeller (48) with the structure of PDB 6CUD as the template. The small-molecule conformations of M085 and GSK1702934A were prepared using LigPrep (49). The docking program Glide (50) was employed to dock M085 or GSK1702934A into the potential binding sites. The grid for the protein was set to 30 Å, and the extra precision (XP) docking mode was selected in *in silico* docking. For Induce-Fit-Docking, all procedures including protein preparation, refinement, grid generation, and docking were carried out using the default parameters. The threshold for rejecting minimized poses was 0.5 kcal/mol. Docking scores and M085/GSK1702934A-residue interaction scores were summarized, sorted, and then plotted using Maestro (51, 52).

Conventional molecular dynamic (CMD) simulations and metadynamics (MetaD) simulations

According to our previous description (51, 53), all MD simulations were performed at a constant number of particles, constant pressure and temperature, and periodic boundary conditions using program DESMOND, which uses a particular "neutral territory"method to efficiently exploit a high degree of computational parallelism (54). The default OPLS_2005 force field was used for hTRPC6, ions, and M085/GSK1702934A. The complexes of hTRPC6/M085 and hTRPC6/GSK1702934A were used as the initial structures for MD simulations (54). Using the large 1-palmitoyl-2-oleoyl-sn-glycero-3-phosphatidylcholine (POPC, 300 K) bilayer provided in DESMOND's System Builder (54), a suitable membrane system was generated in which the TM domain of hTRPC6 could be embedded. The hTRPC6/POPC system is dissolved in simple point charge (SPC) water molecules. Counter ions were then added to compensate for the net negative charge of the system. NaCl (150 mM) was added to the simulation box to represent the background salt under physiological conditions. The DESMOND default relaxation protocol was applied to each system prior to the simulation run. (1) 100 ps simulations in the NVT ensemble with Brownian kinetics using a temperature of 10 K with solute heavy atoms constrained; (2) 12 ps simulations in the NVT ensemble using a Berendsen thermostat with a temperature of 10 K and small-time steps with solute heavy atoms constrained; (3) 12 ps simulations in the NPT ensemble using a Berendsen thermostat and barostat for 12 ps simulations at 10 K and 1 atm, with solute heavy atoms constrained; (4) 12 ps simulations in the NPT ensemble using a Berendsen thermostat and barostat at 300 K and 1 atm with solute heavy atoms constrained; (5) 24 ps simulations in the NPT ensemble using a Berendsen thermostat and barostat at 300 K and 1 atm without constraint. After equilibration, the MD simulations were performed for 100 to 500 ns. Long-range electrostatic interactions were computed using a Smooth Particle Mesh Ewald method. The trajectory recording interval was set to 200 ps and other default parameters were used during CMD simulation runs. The Simulation Interaction Diagram (SID) module in DESMOND was used for exploring the interaction analysis between M085 (or GSK1702934A) and hTRPC6, and the r.m.s (root-mean-square) fluctuations (RMSF) analysis of protein and ligand.

MetaD simulation (55–57) was also conducted by program DESMOND (54) with a constant number of particles, pressure (1 bar) and temperature (300 K) and periodic boundary conditions by using Nose–Hoover chain Thermostat and Martyna–Tobias–Klein Barostat methods. The height and width of the Gaussian and the interval were set to 0.12 kca/mol, 0.05 Å and 0.09 ps, respectively. Before the simulation, the built systems were relaxed by using the protocol of DESMOND in the following sequence: (1) NVT ensemble with Brownian dynamics for 100 ps at 10 K with small time step, and solute heavy atom restrained; (2) NVT ensemble using Berendsen thermostat for 12 ps at 10 K with small time step, and solute heavy atom restrained; (3) NPT ensemble using a Berendsen thermostat and barostat for 12 ps at 10 K and 1 atm with solute heavy atom restrained; (4) NPT ensemble using a Berendsen for 12 ps at 300 K and 1 atm with solute heavy atom restrained; (5) NPT ensemble using a Berendsen for 24 ps at 300 K and 1 atm with no restraints. After the relaxation, the metadynamics runs were protracted for ∼30,000 to 60,000 ps until they showed free diffusivity along the defined collective variables (CVs), which indicates the convergence of metadynamics runs. This criterion was chosen according to the guidelines of assessing the accuracy of metadynamics runs (57). The surface sum of free energy and Gaussians were calculated using the metadynamics analysis tool in DESMOMD (34, 51).

All simulations were run on DELL T7910 graphic working station (with NVIDA Tesla K40C-GPU). Preparation, analysis, and visualization were performed on a 12-CPU CORE DELL T7500 graphic working station.

Electrophysiology

As we described previously (53, 58), whole-cell recordings were performed at room temperature (23 °C ± 2 deg. C) using a voltage clamp under a conventional whole-cell configuration. The pipettes were pulled from glass capillaries through two-stage puller (Narishige PC-10) and filled in a general intracellular solution containing (in mM): 110 CsCl, 10 HEPES, 10 BAPTA, 1 $MgCl_2$, 4.77 $CaCl_2$, pH adjusted to 7.2 with HCl (400 nM free Ca^{2+}) (10), and a resistance varied between 3 and 5 MΩ. Membrane currents were measured with an Axon 200B patch-clamp amplifier (Molecular Devices). Current signals were sampled at 10 kHz and filtered at 2 kHz and analyzed by pClamp 10 (Molecular Devices). The bath solution containing (in mM): 140 NaCl, 5 KCl, 2 $CaCl_2$, 1 $MgCl_2$, 10 glucose, and 10 HEPES, pH adjusted to 7.4 with Tris-base (10). During gap-free recordings, the membrane potential was held at −60 mV and the M085 or GSK1702934A solution was applied with the Y-tube. Single-channel recordings or macro-patch using outside-out or inside-out configurations were carried out in HEK293 cells at room temperature (23 °C ± 2 deg. C) 24 to 48 h after transfection and recording electrodes were drawn from borosilicate glass (World Precision Instruments, Inc). The borosilicate glass was polished to produce resistance about 8 to 12 megohms and the holding potential was set at −60 mV. The external solution and internal solutions are the same as those of whole-cell recordings. Currents were recorded at 50 kHz with 2 kHz filter and a low-pass filtered at 300 Hz, using the AxonPatch 200B amplifier in conjunction with pClamp 10.0 software (Molecular Device).

Surface expression of TRPC6

Cell surface biotinylation and western blotting were performed as per the previously described method (58). Briefly, mTRPC6 or its mutants were expressed in HEK-293 cells and washed in chilled PBS, then bathed in solution containing sulfo-NHS-LC-biotin, and the reaction was stopped by incubating the cells with glycine (20 mM) in PBS. Cells were then collected and lysed with RIPA buffer. The biotinylated proteins were separated from the intracellular protein fraction by agarose resin attached to NeutrAvidin, followed by incubation overnight and subsequent centrifugation. The resin was then washed and the bound proteins were eluted with boiling SDS sample buffer, while 10% volume of the supernatant was diluted as the total protein fraction. The remaining lysate was incubated with NeutrAvidin agarose resin at 4 °C overnight, and then the resin was washed several times with chilled PBS. Protein samples for biotinylation assays were analyzed by Western blotting. All samples and protein markers were separated on SDS-polyacrylamide gels (10%) and transferred to polyvinylidene difluoride (PVDF) membranes. The samples were incubated with anti-EE-tag (1:1000) or anti-GAPDH (1:1000) antibodies overnight at 4 °C, followed by appropriate HRP-conjugated secondary antibodies to EE-tag or GAPDH, and finally exposed to ECL solution (Thermo) and an automated chemiluminescence-fluorescence image analysis system (Tanon 5200, Multi) for 1 to 3 min for visualization. Analysis of protein expression was repeated by at least four independent experiments.

Data analysis

The results are expressed as the means ± SD. Statistical significance between different groups was determined using the Student's t test or Bonferroni's multiple comparisons test (ANOVA, more than two groups), where $p < 0.05$ (*) or $p < 0.01$ (**) was considered significant. By measuring currents in response to different concentrations of M085 and GSK1702934A to obtain the concentration–response relationships for M085 and GSK1702934A activation of wild-type or mutated channels, respectively. Unless otherwise noted, data were obtained from at least three batches of different transfected cells. The data were fitted to the Hill equation, $I/I_{max} = 1/[1 + (EC_{50}/[\text{M085 or GSK1702934A}])^n]$, where I is the normalized current at a given concentration of M085 or GSK1702934A, I_{max} is the maximum normalized current, EC_{50} is the concentration of M085/GSK1702934A yielding a current that is half of the maximum, and n is the Hill coefficient.

Data availability

All data are contained within the manuscript.

Author contributions—Y.-T. L. and Y. Y. conceptualization; J. W., Y.-T. L., and Y. Y. data curation; P.-L. Y., Y.-T. L., and Y. Y. formal analysis; W.-H. W., Y.-T. L., and Y. Y. funding acquisition; P.-L. Y.,

Y.-T. L., and Y. Y. investigation; J. W., W.-H. W., M. X. Z., P.-W. L., Y.-T. L., and Y. Y. methodology; X.-H. L., Z.-H. X., C.-Z. L., C.-R. G., Y.-T. L., and Y. Y. project administration; P. C., M. X. Z., P.-W. L., Z.-H. X., C.-R. G., Y.-T. L., and Y. Y. resources; P.-L. Y., X.-F. M., Y.-F. J., Y.-T. L., and Y. Y. software; X.-H. L., J. W., W.-H. W., P. C., Y.-T. L., and Y. Y. supervision; P.-L. Y., J. W., B.-Y. Z., C.-R. G., Y.-T. L., and Y. Y. validation; P.-L. Y., X.-F. M., Y.-T. L., and Y. Y. visualization; P.-L. Y., Y.-T. L., and Y. Y. writing—original draft; Y.-T. L. and Y. Y. writing—review and editing.

Funding and additional information—This study was supported with funds from the Natural Science Foundation of Jiangsu Province (BK20202002 to Y. Y.), National Natural Science Foundation of China with grant numbers 32000869 (J. W.), 81902480 (W.-H. W.), 31570832 (Y. Y.) and 31971146 (Y. Y.), Innovation and Entrepreneurship Talent Program of Jiangsu Province (Y. Y. and J. W.), State Key Laboratory of Utilization of Woody Oil Resource with grant number 2019XK2002 (C.-Z. L.), Hunan Provincial Natural Science Foundation of China (2018JJ1012 to Y.-T. L.), Guangxi Funds for Distinguished Experts (Y. Y.), and "Xing Yao" Leading Scholars of China Pharmaceutical University (2021) (Y. Y).

Conflict of interest—The authors declare that they have no conflicts of interest with the contents of this article.

Abbreviations—The abbreviations used are: CMD, conventional molecular dynamics; cryo-EM, cryo-electron microscopy; DTNB, 5,5′-dithiobis (2-nitrobenzoic acid); ECD, extracellular domain; MetaD, metadynamics; PH, pore helix; TM, transmembrane; TNB, thiobenzene (2-nitrobenzoic acid); TRPC, transient receptor potential canonical; WT, wild-type.

References

1. Gualdani, R., and Gailly, P. (2020) How TRPC channels modulate hippocampal function. *Int. J. Mol. Sci.* **21**, 3915
2. Yamaguchi, Y., Iribe, G., Nishida, M., and Naruse, K. (2017) Role of TRPC3 and TRPC6 channels in the myocardial response to stretch: Linking physiology and pathophysiology. *Prog. Biophys. Mol. Biol.* **130**, 264–272
3. Mori, M. X., Itsuki, K., Hase, H., Sawamura, S., Kurokawa, T., Mori, Y., and Inoue, R. (2015) Dynamics of receptor-operated Ca(2+) currents through TRPC channels controlled via the PI(4,5)P2-PLC signaling pathway. *Front. Pharmacol.* **6**, 22
4. Hang, P., Zhao, J., Cai, B., Tian, S., Huang, W., Guo, J., Sun, C., Li, Y., and Du, Z. (2015) Brain-derived neurotrophic factor regulates TRPC3/6 channels and protects against myocardial infarction in rodents. *Int. J. Biol. Sci.* **11**, 536–545
5. Sabourin, J., Le Gal, L., Saurwein, L., Haefliger, J. A., Raddatz, E., and Allagnat, F. (2015) Store-operated Ca2+ entry mediated by Orai1 and TRPC1 participates to insulin secretion in rat β-cells. *J. Biol. Chem.* **290**, 30530–30539
6. Qiu, J., Wagner, E. J., Rønnekleiv, O. K., and Kelly, M. J. (2018) Insulin and leptin excite anorexigenic pro-opiomelanocortin neurones via activation of TRPC5 channels. *J. Neuroendocrinol.* **30**, 10
7. Winn, M. P., Conlon, P. J., Lynn, K. L., Farrington, M. K., Creazzo, T., Hawkins, A. F., Daskalakis, N., Kwan, S. Y., Ebersviller, S., Burchette, J. L., Pericak-Vance, M. A., Howell, D. N., Vance, J. M., and Rosenberg, P. B. (2005) A mutation in the TRPC6 cation channel causes familial focal segmental glomerulosclerosis. *Science* **308**, 1801–1804
8. Julius, D. (2013) TRP channels and pain. *Annu. Rev. Cell Dev. Biol.* **29**, 355–384
9. Gaunt, H. J., Vasudev, N. S., and Beech, D. J. (2016) Transient receptor potential canonical 4 and 5 proteins as targets in cancer therapeutics. *Eur. Biophys. J.* **45**, 611–620
10. Qu, C., Ding, M., Zhu, Y., Lu, Y., Du, J., Miller, M., Tian, J., Zhu, J., Xu, J., Wen, M., Er-Bu, A., Wang, J., Xiao, Y., Wu, M., McManus, O. B., *et al.* (2017) Pyrazolopyrimidines as potent stimulators for transient receptor potential canonical 3/6/7 channels. *J. Med. Chem.* **60**, 4680–4692
11. Xu, X., Lozinskaya, I., Costell, M., Lin, Z., Ball, J. A., Bernard, R., Behm, D. J., Marino, J. P., and Schnackenberg, C. G. (2013) Characterization of small molecule TRPC3 and TRPC6 agonist and antagonists. *Biophys. J.* **104**, 454
12. Doleschal, B., Primessnig, U., Wölkart, G., Wolf, S., Schernthaner, M., Lichtenegger, M., Glasnov, T. N., Kappe, C. O., Mayer, B., Antoons, G., Heinzel, F., Poteser, M., and Groschner, K. (2015) TRPC3 contributes to regulation of cardiac contractility and arrhythmogenesis by dynamic interaction with NCX1. *Cardiovasc. Res.* **106**, 163–173
13. Liu, H., Yang, L., Chen, K. H., Sun, H. Y., Jin, M. W., Xiao, G. S., Wang, Y., and Li, G. R. (2016) SKF-96365 blocks human ether-à-go-go-related gene potassium channels stably expressed in HEK 293 cells. *Pharmacol. Res.* **104**, 61–69
14. Sabourin, J., Bartoli, F., Antigny, F., Gomez, A. M., and Benitah, J. P. (2016) Transient receptor potential canonical (TRPC)/Orai1-dependent store-operated Ca2+ channels: New targets of aldosterone in cardiomyocytes. *J. Biol. Chem.* **291**, 13394–13409
15. Lin, B. L., Matera, D., Doerner, J. F., Zheng, N., Del Camino, D., Mishra, S., Bian, H., Zeveleva, S., Zhen, X., Blair, N. T., Chong, J. A., Hessler, D. P., Bedja, D., Zhu, G., Muller, G. K., *et al.* (2019) *In vivo* selective inhibition of TRPC6 by antagonist BI 749327 ameliorates fibrosis and dysfunction in cardiac and renal disease. *Proc. Natl. Acad. Sci. U. S. A.* **116**, 10156–10161
16. Kiyonaka, S., Kato, K., Nishida, M., Mio, K., Numaga, T., Sawaguchi, Y., Yoshida, T., Wakamori, M., Mori, E., Numata, T., Ishii, M., Takemoto, H., Ojida, A., Watanabe, K., Uemura, A., *et al.* (2009) Selective and direct inhibition of TRPC3 channels underlies biological activities of a pyrazole compound. *Proc. Natl. Acad. Sci. U. S. A.* **106**, 5400–5405
17. Koenig, S., Schernthaner, M., Maechler, H., Kappe, C. O., Glasnov, T. N., Hoefler, G., Braune, M., Wittchow, E., and Groschner, K. (2013) A TRPC3 blocker, ethyl-1-(4-(2,3,3-trichloroacrylamide)phenyl)-5-(trifluoromethyl)-1H-pyrazole-4-carboxylate (Pyr3), prevents stent-induced arterial remodeling. *J. Pharmacol. Exp. Ther.* **344**, 33–40
18. Sawamura, S., Hatano, M., Takada, Y., Hino, K., Kawamura, T., Tanikawa, J., Nakagawa, H., Hase, H., Nakao, A., Hirano, M., Rotrattanadumrong, R., Kiyonaka, S., Mori, M. X., Nishida, M., Hu, Y., *et al.* (2016) Screening of transient receptor potential canonical channel activators identifies novel neurotrophic piperazine compounds. *Mol. Pharmacol.* **89**, 348–363
19. Dryer, S. E., Roshanravan, H., and Kim, E. Y. (2019) TRPC channels: Regulation, dysregulation and contributions to chronic kidney disease. *Biochim. Biophys. Acta Mol. Basis Dis.* **1865**, 1041–1066
20. Wu, Y. L., Xie, J., An, S. W., Oliver, N., Barrezueta, N. X., Lin, M. H., Birnbaumer, L., and Huang, C. L. (2017) Inhibition of TRPC6 channels ameliorates renal fibrosis and contributes to renal protection by soluble klotho. *Kidney Int.* **91**, 830–841
21. Jiang, H. N., Zeng, B., Chen, G. L., Lai, B., Lu, S. H., and Qu, J. M. (2016) Lipopolysaccharide potentiates endothelin-1-induced proliferation of pulmonary arterial smooth muscle cells by upregulating TRPC channels. *Biomed. Pharmacother.* **82**, 20–27
22. He, D. X., and Ma, X. (2016) Transient receptor potential channel C5 in cancer chemoresistance. *Acta Pharmacol. Sin.* **37**, 19–24
23. Jardin, I., and Rosado, J. A. (2016) STIM and calcium channel complexes in cancer. *Biochim. Biophys. Acta* **1863**, 1418–1426
24. Chen, X., Sooch, G., Demaree, I. S., White, F. A., and Obukhov, A. G. (2020) Transient receptor potential canonical (TRPC) channels: Then and now. *Cells* **9**, 1983
25. Hofmann, T., Obukhov, A. G., Schaefer, M., Harteneck, C., Gudermann, T., and Schultz, G. (1999) Direct activation of human TRPC6 and TRPC3 channels by diacylglycerol. *Nature* **397**, 259–263
26. Liu, C. H., Gong, Z., Liang, Z. L., Liu, Z. X., Yang, F., Sun, Y. J., Ma, M. L., Wang, Y. J., Ji, C. R., Wang, Y. H., Wang, M. J., Cui, F. A., Lin, A., Zheng, W. S., He, D. F., *et al.* (2017) Arrestin-biased AT1R agonism induces acute catecholamine secretion through TRPC3 coupling. *Nat. Commun.* **8**, 14335

27. Kanki, H., Kinoshita, M., Akaike, A., Satoh, M., Mori, Y., and Kaneko, S. (2001) Activation of inositol 1,4,5-trisphosphate receptor is essential for the opening of mouse TRP5 channels. *Mol. Pharmacol.* **60**, 989–998
28. Bai, Y., Yu, X., Chen, H., Horne, D., White, R., Wu, X., Lee, P., Gu, Y., Ghimire-Rijal, S., Lin, D. C., and Huang, X. (2020) Structural basis for pharmacological modulation of the TRPC6 channel. *Elife* **9**, e53311
29. Lichtenegger, M., Tiapko, O., Svobodova, B., Stockner, T., Glasnov, T. N., Schreibmayer, W., Platzer, D., de la Cruz, G. G., Krenn, S., Schober, R., Shrestha, N., Schindl, R., Romanin, C., and Groschner, K. (2018) An optically controlled probe identifies lipid-gating fenestrations within the TRPC3 channel. *Nat. Chem. Biol.* **14**, 396–404
30. Barducci, A., Bussi, G., and Parrinello, M. (2008) Well-tempered metadynamics: A smoothly converging and tunable free-energy method. *Phys. Rev. Lett.* **100**, 020603
31. Lakkaniga, N. R., Balasubramaniam, M., Zhang, S., Frett, B., and Li, H. Y. (2019) Structural characterization of the aurora kinase B "DFG-flip" using metadynamics. *AAPS J.* **22**, 14
32. Laio, A., and Parrinello, M. (2002) Escaping free-energy minima. *Proc. Natl. Acad. Sci. U. S. A.* **99**, 12562–12566
33. Fu, H., Chen, H., Wang, X., Chai, H., Shao, X., Cai, W., and Chipot, C. (2020) Finding an optimal pathway on a multidimensional free-energy landscape. *J. Chem. Inf. Model.* **60**, 5366–5374
34. Wang, J., Wang, Y., Cui, W. W., Huang, Y., Yang, Y., Liu, Y., Zhao, W. S., Cheng, X. Y., Sun, W. S., Cao, P., Zhu, M. X., Wang, R., Hattori, M., and Yu, Y. (2018) Druggable negative allosteric site of P2X3 receptors. *Proc. Natl. Acad. Sci. U. S. A.* **115**, 4939–4944
35. Dietrich, A., Mederos y Schnitzler, M., Kalwa, H., Storch, U., and Gudermann, T. (2005) Functional characterization and physiological relevance of the TRPC3/6/7 subfamily of cation channels. *Naunyn Schmiedebergs Arch. Pharmacol.* **371**, 257–265
36. Mandelman, D., Jamal, J., and Poulos, T. L. (1998) Identification of two electron-transfer sites in ascorbate peroxidase using chemical modification, enzyme kinetics, and crystallography. *Biochemistry* **37**, 17610–17617
37. Niu, Y. Y., Yang, Y., Liu, Y., Huang, L. D., Yang, X. N., Fan, Y. Z., Cheng, X. Y., Cao, P., Hu, Y. M., Li, L., Lu, X. Y., Tian, Y., and Yu, Y. (2016) Exploration of the peptide recognition of an amiloride-sensitive FMRFamide peptide-gated sodium channel. *J. Biol. Chem.* **291**, 7571–7582
38. Schmiege, P., Fine, M., Blobel, G., and Li, X. (2017) Human TRPML1 channel structures in open and closed conformations. *Nature* **550**, 366–370
39. Wright, D. J., Simmons, K. J., Johnson, R. M., Beech, D. J., Muench, S. P., and Bon, R. S. (2020) Human TRPC5 structures reveal interaction of a xanthine-based TRPC1/4/5 inhibitor with a conserved lipid binding site. *Commun. Biol.* **3**, 704
40. Vinayagam, D., Mager, T., Apelbaum, A., Bothe, A., Merino, F., Hofnagel, O., Gatsogiannis, C., and Raunser, S. (2018) Electron cryo-microscopy structure of the canonical TRPC4 ion channel. *Elife* **7**, e36615
41. Bohlen, C. J., Priel, A., Zhou, S., King, D., Siemens, J., and Julius, D. (2010) A bivalent tarantula toxin activates the capsaicin receptor, TRPV1, by targeting the outer pore domain. *Cell* **141**, 834–845
42. Tang, Q., Guo, W., Zheng, L., Wu, J. X., Liu, M., Zhou, X., Zhang, X., and Chen, L. (2018) Structure of the receptor-activated human TRPC6 and TRPC3 ion channels. *Cell Res.* **28**, 746–755
43. Fan, C., Choi, W., Sun, W., Du, J., and Lü, W. (2018) Structure of the human lipid-gated cation channel TRPC3. *Elife* **7**, e36852
44. Azumaya, C. M., Sierra-Valdez, F., Cordero-Morales, J. F., and Nakagawa, T. (2018) Cryo-EM structure of the cytoplasmic domain of murine transient receptor potential cation channel subfamily C member 6 (TRPC6). *J. Biol. Chem.* **293**, 10381–10391
45. Gowda, G. B., Charanraj, T. P., Kumara, C. S. P., Ramesh, N., and Thomas, S. P. (2014) Synthesis of novel β-aryl-β-(methylthio)acroleins via Vilsmeier–Haack protocol as potential 1,3-dielectrophilic three-carbon building blocks. *Tetrahderon Lett.* **55**, 4475–4479
46. Byre Gowda, G., Kumara, C. S. P., Ramesh, N., Sadashiva, M. P., and Junjappa, H. (2016) Base catalyzed reaction of ethylthioglycolate with β-aryl-β-(methylthio) acroleins: A general method for the synthesis of 2-carbethoxy-5-substituted/4, 5-annulated thiophenes in high overall yields. *Tetrahderon Lett.* **57**, 928–931
47. Friesner, R. A., Murphy, R. B., Repasky, M. P., Frye, L. L., Greenwood, J. R., Halgren, T. A., Sanschagrin, P. C., and Mainz, D. T. (2006) Extra precision glide: Docking and scoring incorporating a model of hydrophobic enclosure for protein-ligand complexes. *J. Med. Chem.* **49**, 6177–6196
48. Sali, A., and Blundell, T. L. (1993) Comparative protein modelling by satisfaction of spatial restraints. *J. Mol. Biol.* **234**, 779–815
49. Gadakar, P. K., Phukan, S., Dattatreya, P., and Balaji, V. N. (2007) Pose prediction accuracy in docking studies and enrichment of actives in the active site of GSK-3beta. *J. Chem. Inf. Model.* **47**, 1446–1459
50. Friesner, R. A., Banks, J. L., Murphy, R. B., Halgren, T. A., Klicic, J. J., Mainz, D. T., Repasky, M. P., Knoll, E. H., Shelley, M., Perry, J. K., Shaw, D. E., Francis, P., and Shenkin, P. S. (2004) Glide: A new approach for rapid, accurate docking and scoring. 1. Method and assessment of docking accuracy. *J. Med. Chem.* **47**, 1739–1749
51. Li, B., Wang, J., Cheng, X., Liu, Y., and Yu, Y. (2018) Molecular mechanism underlying the subtype-selectivity of competitive inhibitor NF110 and its distinct potencies in human and rat P2X3 receptors. *Sci. Bull.* **63**, 1616–1625
52. Huang, L. D., Fan, Y. Z., Tian, Y., Yang, Y., Liu, Y., Wang, J., Zhao, W. S., Zhou, W. C., Cheng, X. Y., Cao, P., Lu, X. Y., and Yu, Y. (2014) Inherent dynamics of head domain correlates with ATP-recognition of P2X4 receptors: Insights gained from molecular simulations. *PLoS One* **9**, e97528
53. Zhao, W. S., Wang, J., Ma, X. J., Yang, Y., Liu, Y., Huang, L. D., Fan, Y. Z., Cheng, X. Y., Chen, H. Z., Wang, R., and Yu, Y. (2014) Relative motions between left flipper and dorsal fin domains favour P2X4 receptor activation. *Nat. Commun.* **5**, 4189
54. Shaw, D. E. (2005) A fast, scalable method for the parallel evaluation of distance-limited pairwise particle interactions. *J. Comput. Chem.* **26**, 1318–1328
55. Laio, A., and Gervasio, F. L. (2008) Metadynamics: A method to simulate rare events and reconstruct the free energy in biophysics, chemistry and material science. *Rep. Prog. Phys.* **71**, 126601
56. Limongelli, V., Bonomi, M., Marinelli, L., Gervasio, F. L., Cavalli, A., Novellino, E., and Parrinello, M. (2010) Molecular basis of cyclooxygenase enzymes (COXs) selective inhibition. *Proc. Natl. Acad. Sci. U. S. A.* **107**, 5411–5416
57. Laio, A., Rodriguez-Fortea, A., Gervasio, F. L., Ceccarelli, M., and Parrinello, M. (2005) Assessing the accuracy of metadynamics. *J. Phys. Chem. B* **109**, 6714–6721
58. Sun, L. F., Liu, Y., Wang, J., Huang, L. D., Yang, Y., Cheng, X. Y., Fan, Y. Z., Zhu, M. X., Liang, H., Tian, Y., Wang, H. S., Guo, C. R., and Yu, Y. (2019) Altered allostery of the left flipper domain underlies the weak ATP response of rat P2X5 receptors. *J. Biol. Chem.* **294**, 19589–19603